MATHEMATICAL MODELLING OF NEMATIC LIQUID CRYSTALS

Joseph R. L. Cousins[1,2]

[1]School of Mathematics and Statistics, University of Glasgow, University Place, Glasgow G12 8QQ, UK
[2]Department of Mathematics and Statistics, University of Strathclyde, 26 Richmond Street, Glasgow G1 1XH, UK

RSE Network Meeting – University of Glasgow – 2nd November 2022

joseph.cousins@strath.ac.uk / joseph.cousins@glasgow.ac.uk

Nottingham Trent University
University of Strathclyde
EPSRC Engineering and Physical Sciences Research Council
University of Glasgow

INTRODUCTION

Brian Duffy and Lindsey Corson

EPSRC project left-to-right: Ian Sage, Akhshay Bhadwal, Joseph Cousins, Nigel Mottram, Carl Brown and Stephen Wilson.

NEMATIC LIQUID CRYSTALS

Liquid crystals are materials that possess additional phases of matter (beyond the well-known phases of solids, liquids and gases) that display crystalline ordering in a liquid phase.

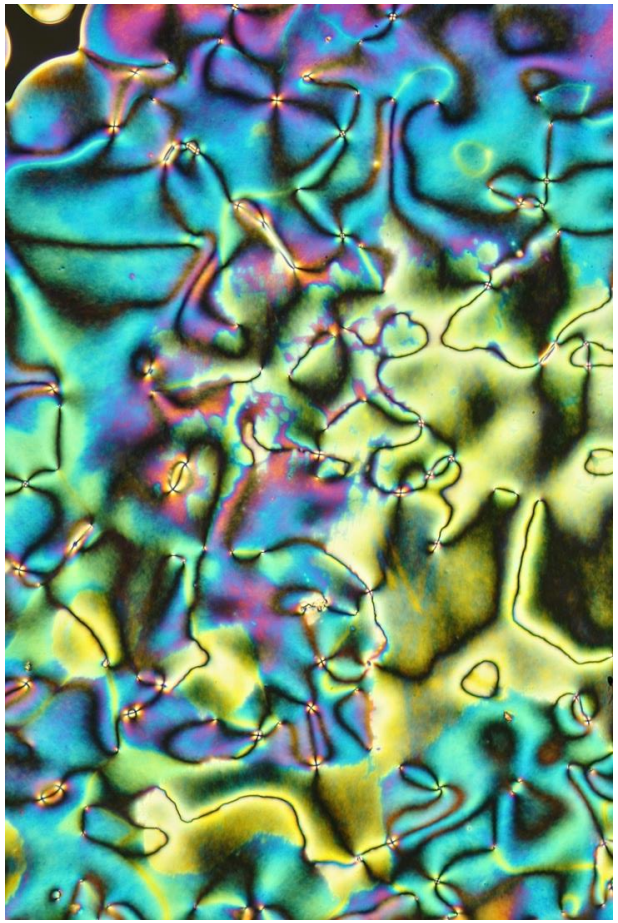

Photograph of the nematic phase viewed under a microscope.
[http://lcmicroscopy.weebly.com/lcphotogallery].

NEMATIC LIQUID CRYSTALS

Liquid crystals are materials that possess additional phases of matter (beyond the well-known phases of solids, liquids and gases) that display crystalline ordering in a liquid phase.

In the nematic liquid crystal (nematic) phase, constituent molecules are rod-like and locally align along a common direction.

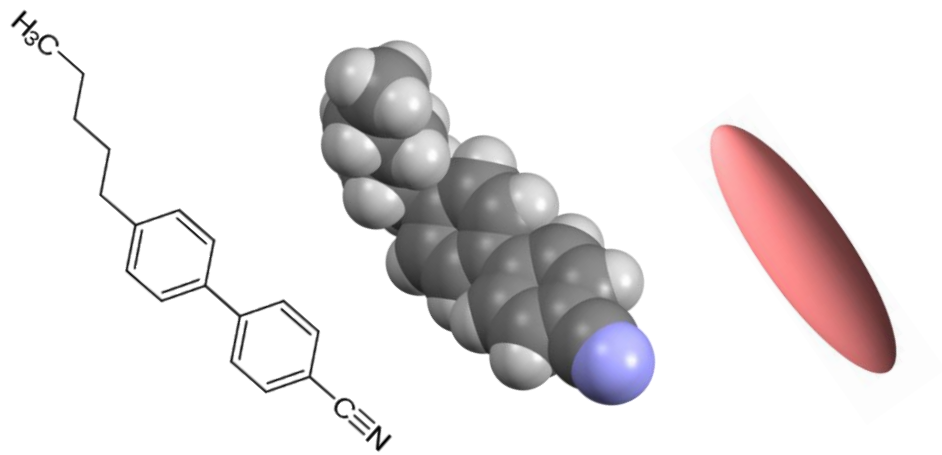

Rod-like molecule of a commonly used nematic called "5CB", which was first synthesised in the UK.
[molecular structure taken from Wikipedia]

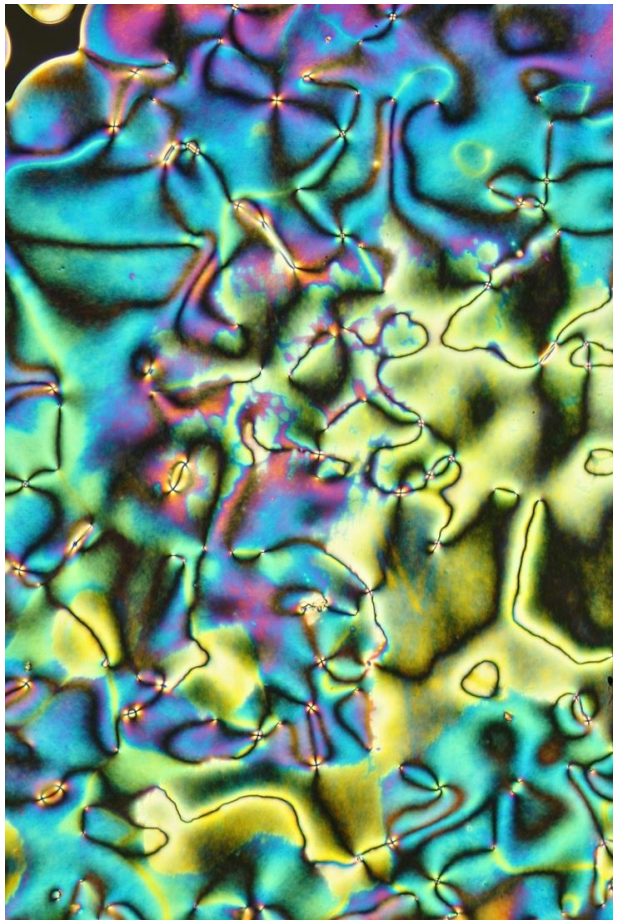

Photograph of the nematic phase viewed under a microscope.
[http://lcmicroscopy.weebly.com/lcphotogallery].

NEMATIC LIQUID CRYSTALS

Liquid crystals are materials that possess additional phases of matter (beyond the well-known phases of solids, liquids and gases) that display crystalline ordering in a liquid phase.

In the nematic liquid crystal (nematic) phase, constituent molecules are rod-like and locally align along a common direction.

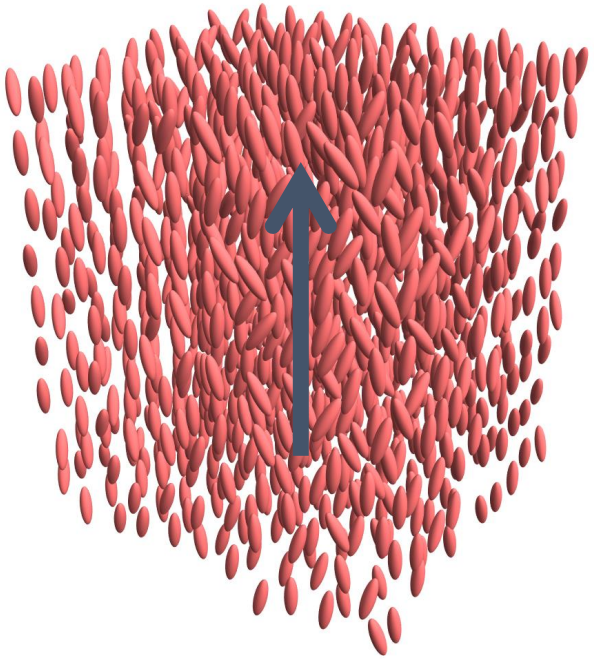

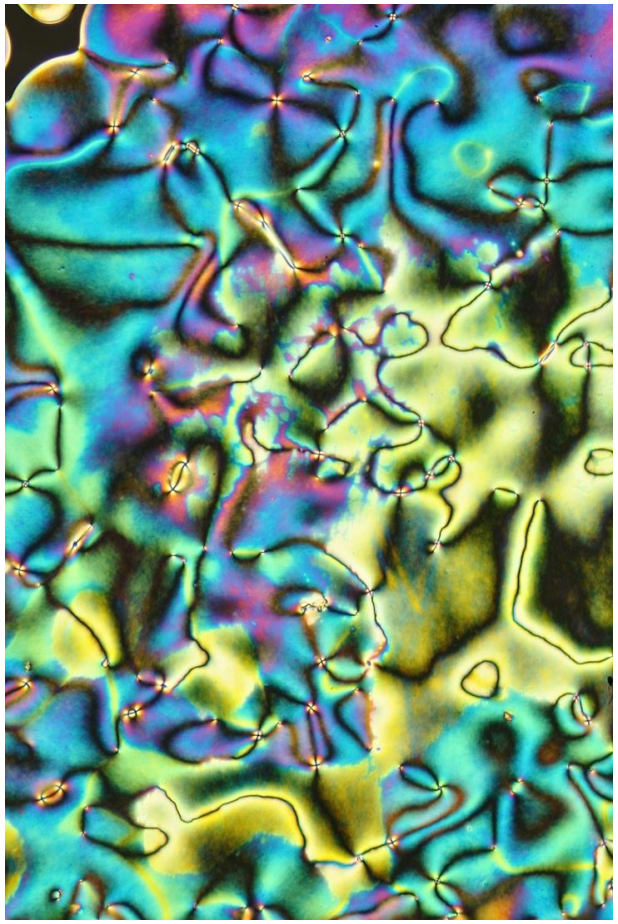

Photograph of the nematic phase viewed under a microscope. [http://lcmicroscopy.weebly.com/lcphotogallery].

DIRECTOR FORMULATION

The average orientation of the nematic molecules is mathematically described by a unit vector called the director ***n***.

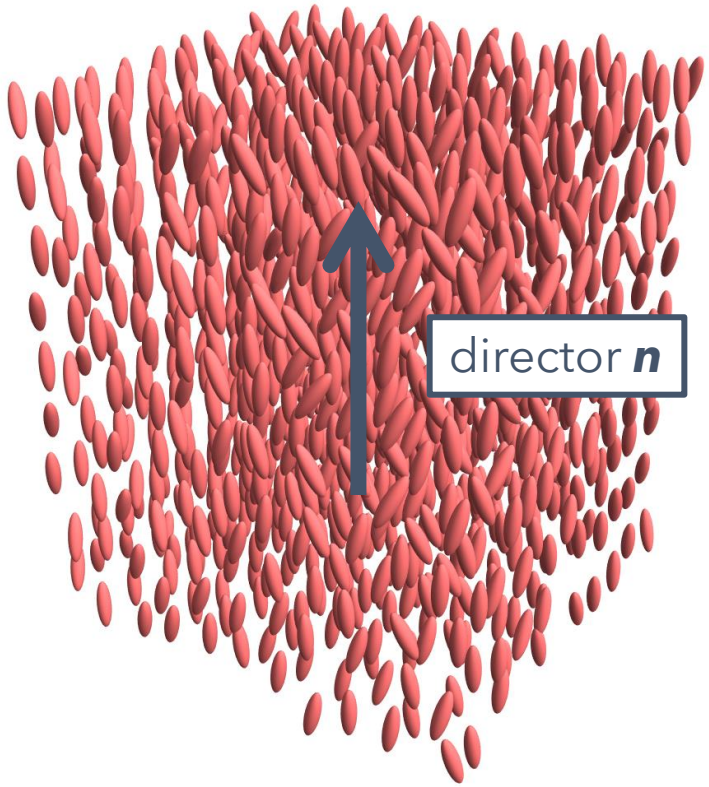

DIRECTOR FORMULATION

The average orientation of the nematic molecules is mathematically described by a unit vector called the director ***n***.

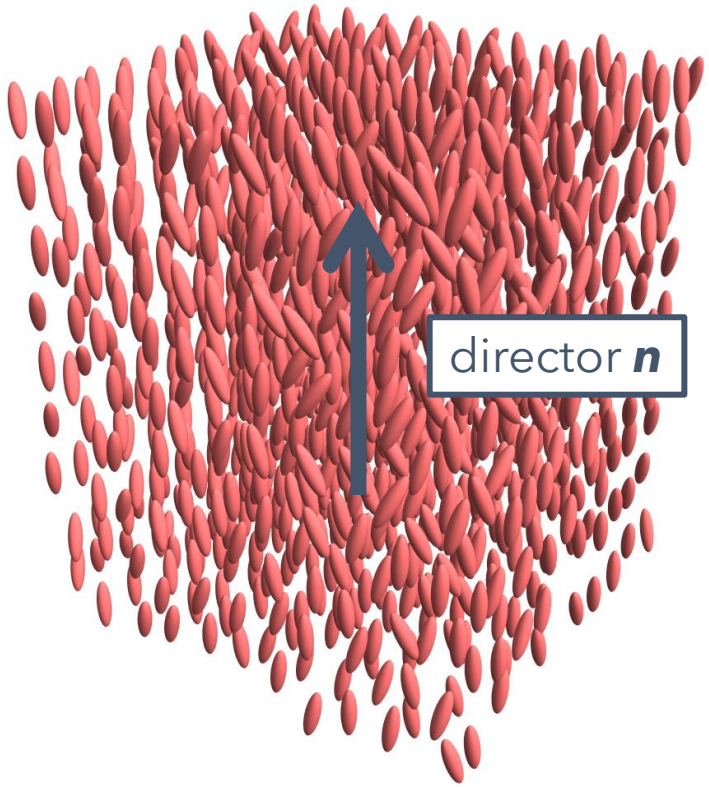

The director formulation allows for a phenomenological theory which can account for anisotropic viscosity, elasticity, surface effects and body forces.

DIRECTOR FORMULATION

The average orientation of the nematic molecules is mathematically described by a unit vector called the director ***n***.

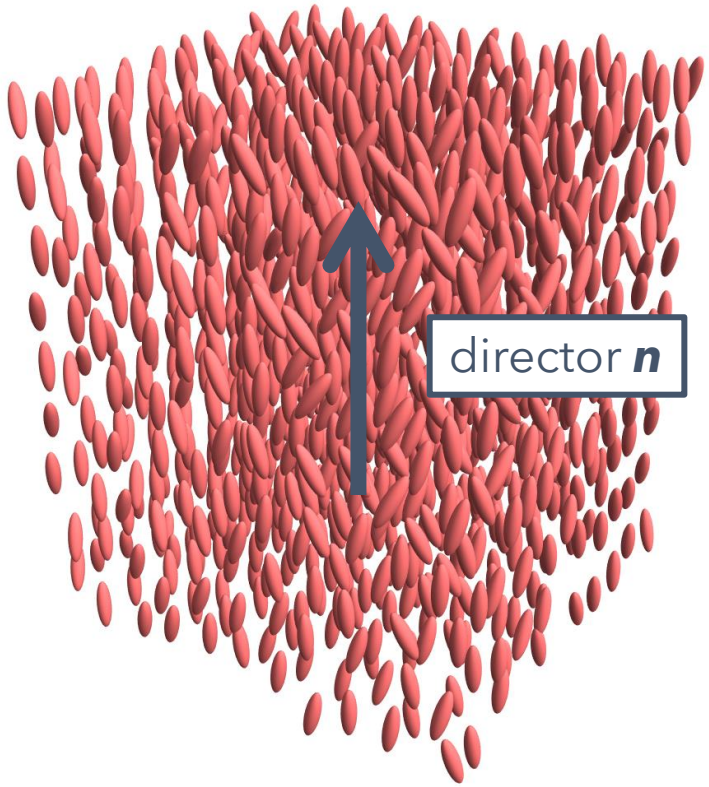

The director formulation allows for a phenomenological theory which can account for anisotropic viscosity, elasticity, surface effects and body forces.

The dynamic continuum theory using the director formulation is known as the Ericksen-Leslie theory.

$$\rho \dot{u}_i = -\frac{\partial}{\partial x_i}(p + W_F) + \tilde{g}_j n_{i,j} + \frac{\partial \tilde{t}_{ij}}{\partial x_j}$$

$$\lambda n_i = \tilde{g}_i + \frac{\partial W_F}{\partial n_i} - \frac{\partial}{\partial x_j}\left(\frac{\partial W_F}{\partial n_{i,j}}\right)$$

Frank Leslie and Jerald Ericksen [Atkin and Sluckin, *Biogr. Mems Fell. R. Soc.* **49** (2003) 315-333]

LIQUID CRYSTALS DISPLAYS

LCDs are now ubiquitous in every aspect of modern life. Televisions, computer monitors, mobile phones and tablets are used every day by most of the world's population.

LIQUID CRYSTALS DISPLAYS

LCDs are now ubiquitous in every aspect of modern life. Televisions, computer monitors, mobile phones and tablets are used every day by most of the world's population.

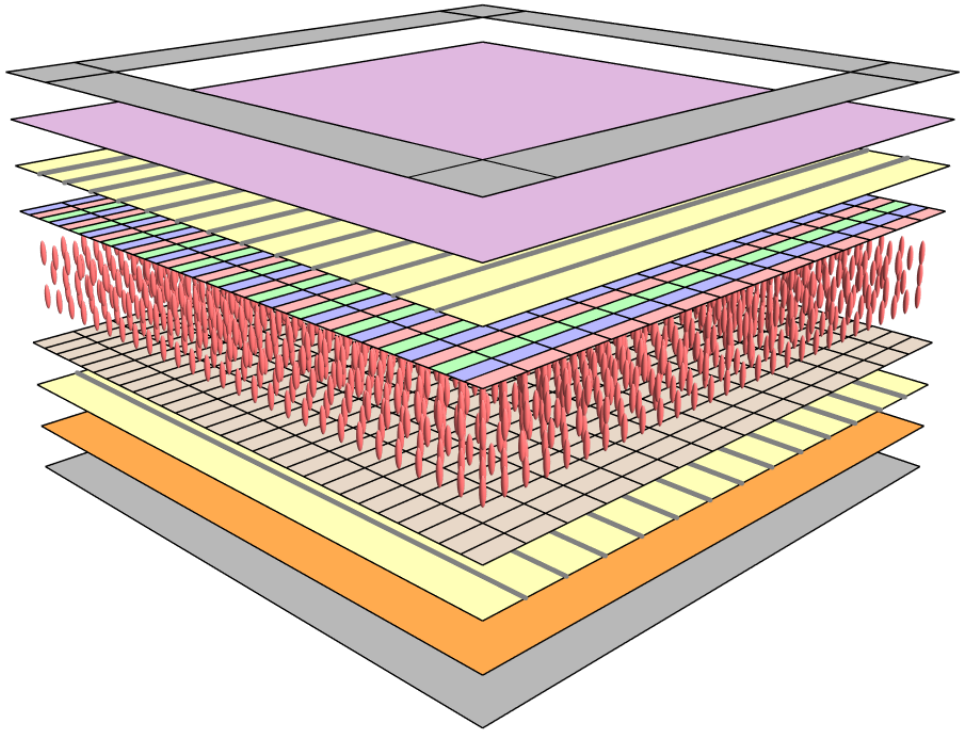

LCD MANUFACTURING

Previously we have worked on the mathematical modelling of LCD manufacturing [1-4].

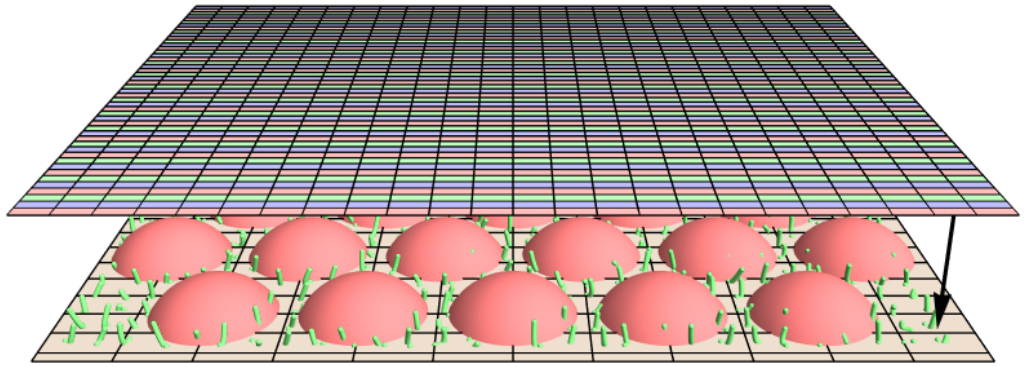

The One Drop Filling method is used to fill displays.

[1] Cousins et al. *Proc. Int. Disp. Workshops,* **25** (2018) LCT8-4.
[2] Cousins et al. *Phys. Fluids*, **31** (2019) 083107.
[3] Cousins et al. *Phys. Rev. E*, **102** (2020) 062703.
[4] Cousins. *PhD Thesis*, University of Strathclyde (2021).

LCD MANUFACTURING

Previously we have worked on the mathematical modelling of LCD manufacturing [1-4].

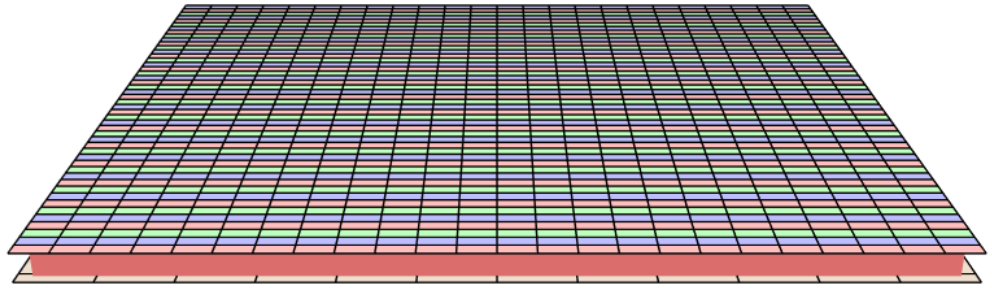

The One Drop Filling method is used to fill displays.

[1] Cousins et al. *Proc. Int. Disp. Workshops,* **25** (2018) LCT8-4.
[2] Cousins et al. *Phys. Fluids*, **31** (2019) 083107.
[3] Cousins et al. *Phys. Rev. E*, **102** (2020) 062703.
[4] Cousins. *PhD Thesis*, University of Strathclyde (2021).

LCD MANUFACTURING

Previously we have worked on the mathematical modelling of LCD manufacturing [1-4].

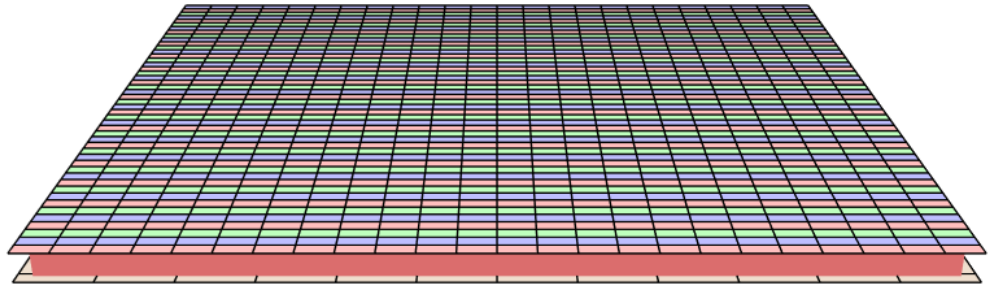

The One Drop Filling method is used to fill displays.

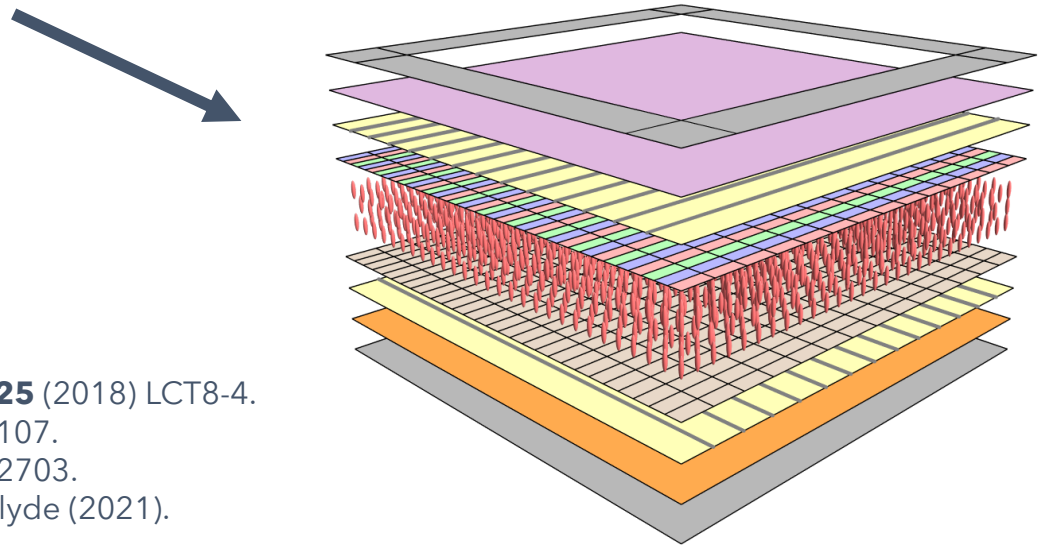

[1] Cousins et al. *Proc. Int. Disp. Workshops,* **25** (2018) LCT8-4.
[2] Cousins et al. *Phys. Fluids*, **31** (2019) 083107.
[3] Cousins et al. *Phys. Rev. E*, **102** (2020) 062703.
[4] Cousins. *PhD Thesis*, University of Strathclyde (2021).

LCD MANUFACTURING

Previously we have worked on the mathematical modelling of LCD manufacturing [1-4].

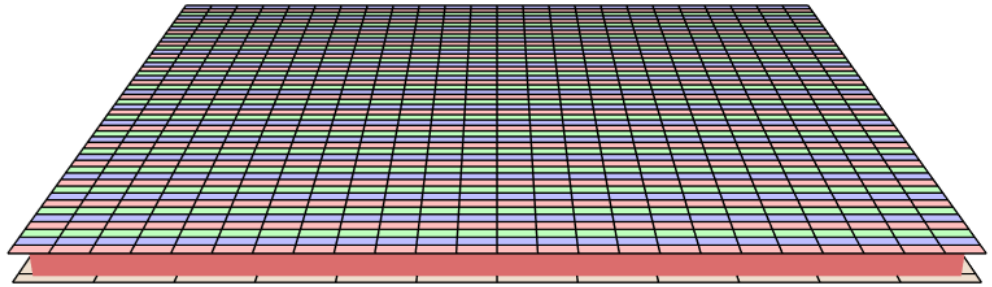

The One Drop Filling method is used to fill displays.

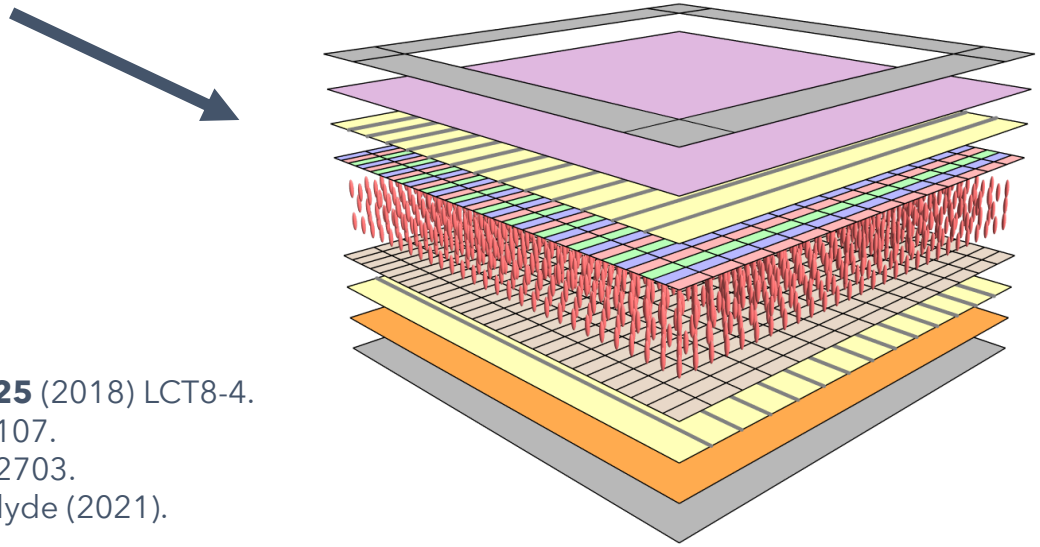

[1] Cousins et al. *Proc. Int. Disp. Workshops,* **25** (2018) LCT8-4.
[2] Cousins et al. *Phys. Fluids*, **31** (2019) 083107.
[3] Cousins et al. *Phys. Rev. E*, **102** (2020) 062703.
[4] Cousins. *PhD Thesis*, University of Strathclyde (2021).

LCD MANUFACTURING

Previously we have worked on the mathematical modelling of LCD manufacturing [1-4].

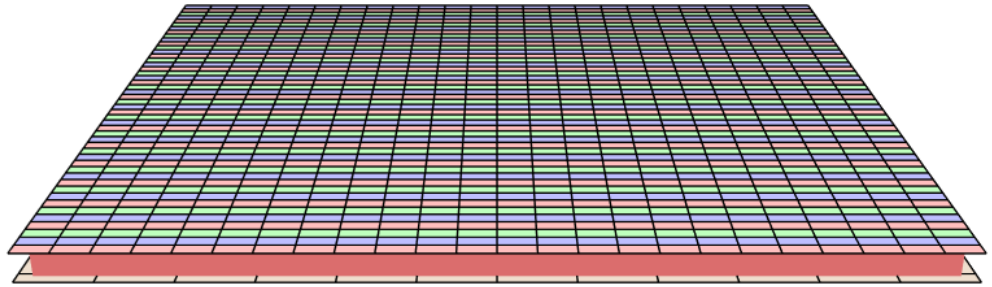

The One Drop Filling method is used to fill displays.

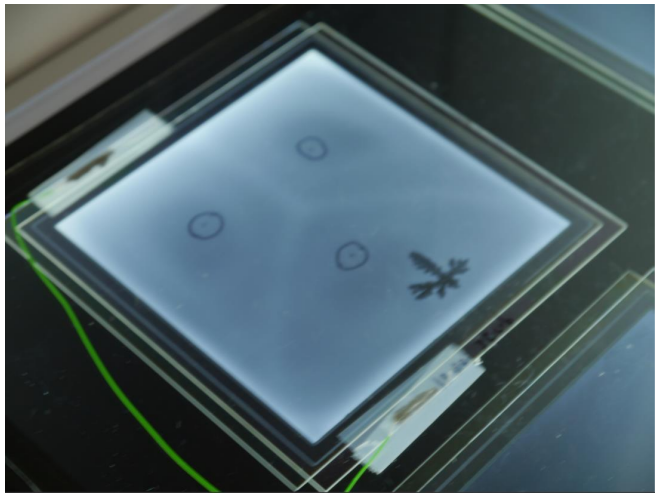

The method is known to produce the *ODF mura* which can degrade the final display product.

[1] Cousins et al. *Proc. Int. Disp. Workshops,* **25** (2018) LCT8-4.
[2] Cousins et al. *Phys. Fluids*, **31** (2019) 083107.
[3] Cousins et al. *Phys. Rev. E*, **102** (2020) 062703.
[4] Cousins. *PhD Thesis*, University of Strathclyde (2021).

UNDERSTANDING THE ODF MURA

Our mathematical analysis shows that flow-driven misalignment of the orientation of the molecules in the substrate alignment layers could play a key role in the formation of ODF mura [1-4].

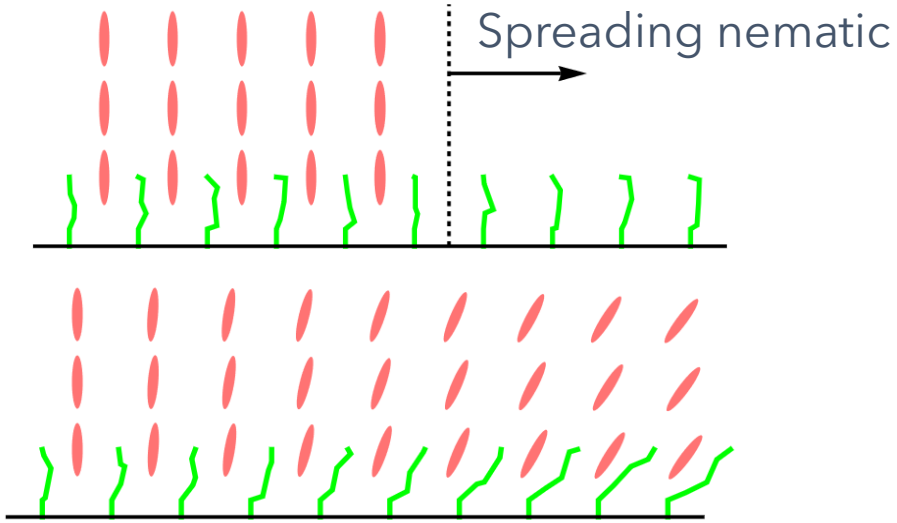

Flow-driven misalignment of the substrate alignment layer

[1] Cousins et al. *Proc. Int. Disp. Workshops,* **25** (2018) LCT8-4.
[2] Cousins et al. *Phys. Fluids*, **31** (2019) 083107.
[3] Cousins et al. *Phys. Rev. E*, **102** (2020) 062703.
[4] Cousins. *PhD Thesis*, University of Strathclyde (2021).

UNDERSTANDING THE ODF MURA

Our mathematical analysis shows that flow-driven misalignment of the orientation of the molecules in the substrate alignment layers could play a key role in the formation of ODF mura [1-4].

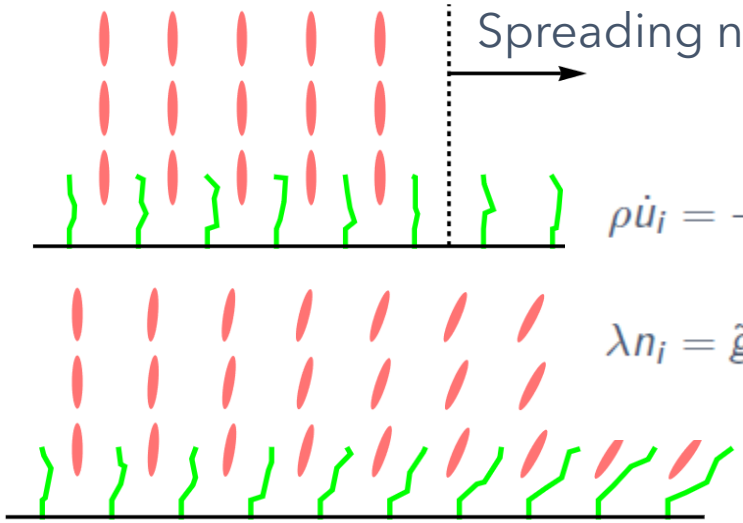

$$\rho \dot{u}_i = -\frac{\partial}{\partial x_i}(p + W_F) + \tilde{g}_j n_{i,j} + \frac{\partial \tilde{t}_{ij}}{\partial x_j}$$

$$\lambda n_i = \tilde{g}_i + \frac{\partial W_F}{\partial n_i} - \frac{\partial}{\partial x_j}\left(\frac{\partial W_F}{\partial n_{i,j}}\right)$$

Flow-driven misalignment of the substrate alignment layer

[1] Cousins et al. *Proc. Int. Disp. Workshops,* **25** (2018) LCT8-4.
[2] Cousins et al. *Phys. Fluids*, **31** (2019) 083107.
[3] Cousins et al. *Phys. Rev. E*, **102** (2020) 062703.
[4] Cousins. *PhD Thesis*, University of Strathclyde (2021).

UNDERSTANDING THE ODF MURA

Our mathematical analysis shows that flow-driven misalignment of the orientation of the molecules in the substrate alignment layers could play a key role in the formation of ODF mura [1-4].

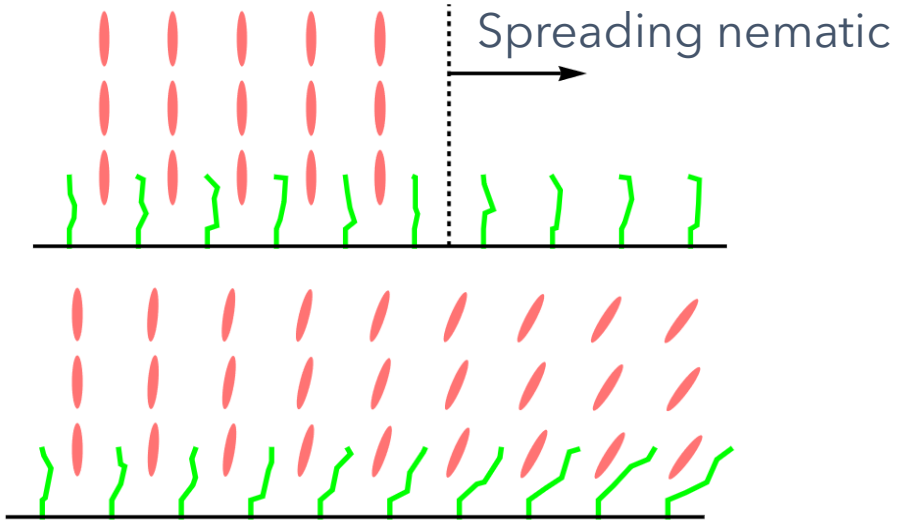

Flow-driven misalignment of the substrate alignment layer

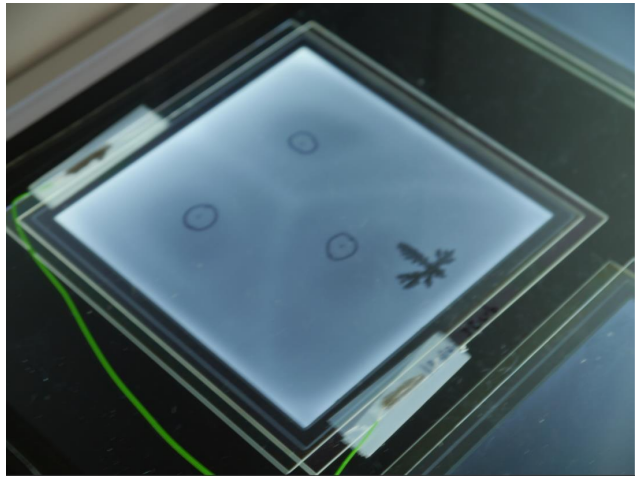

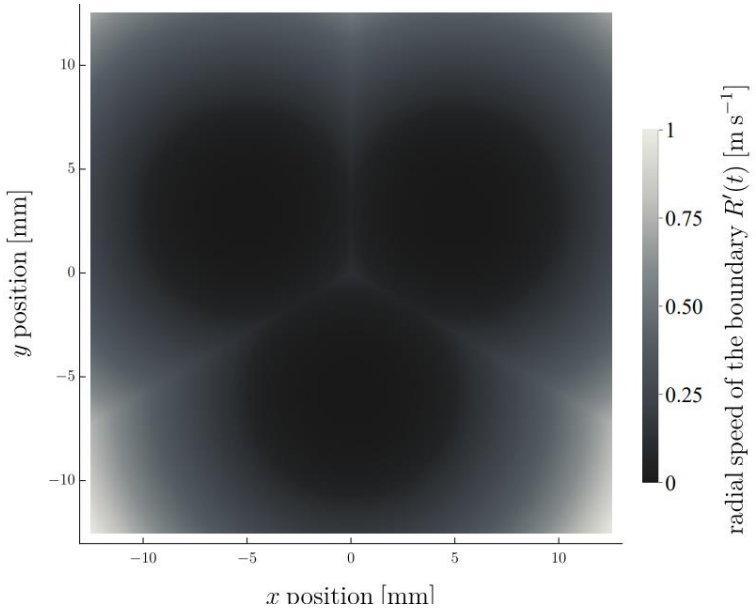

We see a *striking qualitative similarity* for the theoretical prediction for the radial boundary speed of the droplets in the ODF method and the photographs of the ODF mura.

[1] Cousins et al. *Proc. Int. Disp. Workshops,* **25** (2018) LCT8-4.
[2] Cousins et al. *Phys. Fluids*, **31** (2019) 083107.
[3] Cousins et al. *Phys. Rev. E*, **102** (2020) 062703.
[4] Cousins. *PhD Thesis*, University of Strathclyde (2021).

UNDERSTANDING THE ODF MURA

Our mathematical analysis shows that flow-driven misalignment of the orientation of the molecules in the substrate alignment layers could play a key role in the formation of ODF mura [1-4].

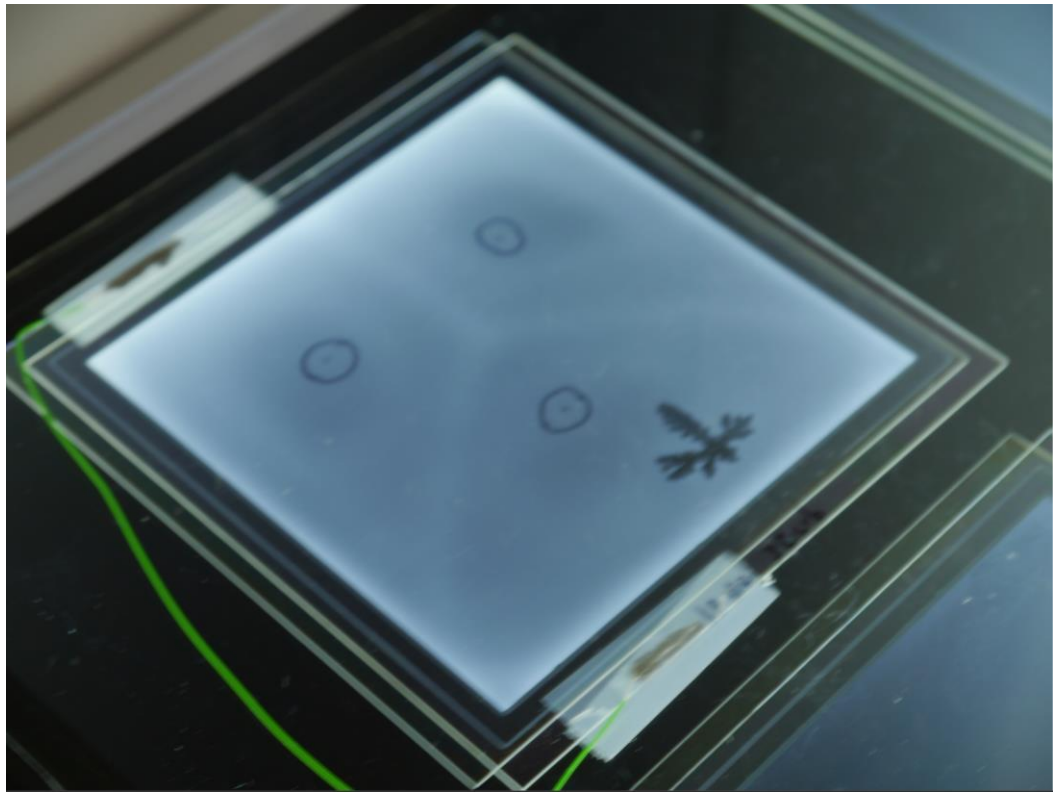

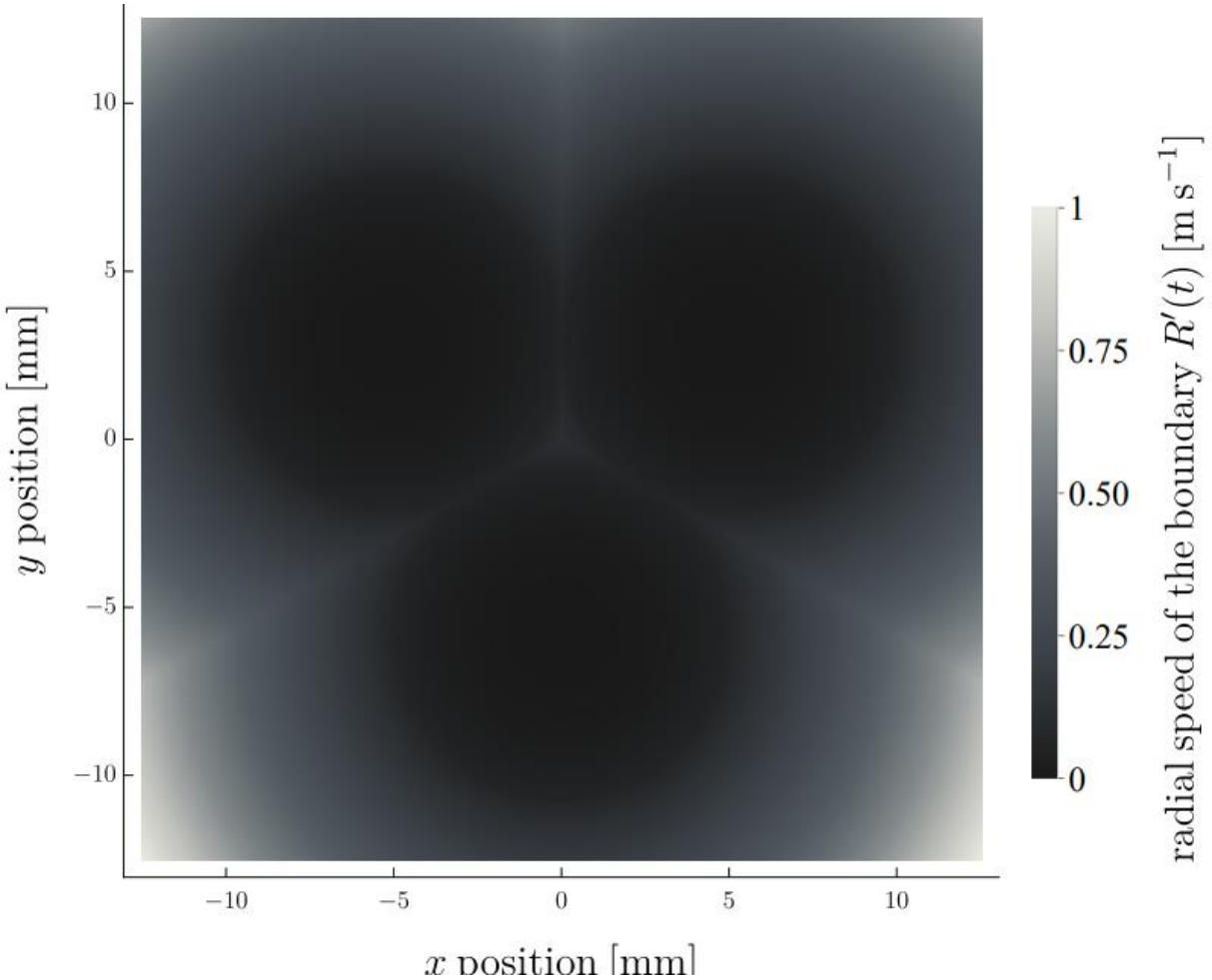

UNDERSTANDING THE ODF MURA

Our mathematical analysis shows that flow-driven misalignment of the orientation of the molecules in the substrate alignment layers could play a key role in the formation of ODF mura [1-4].

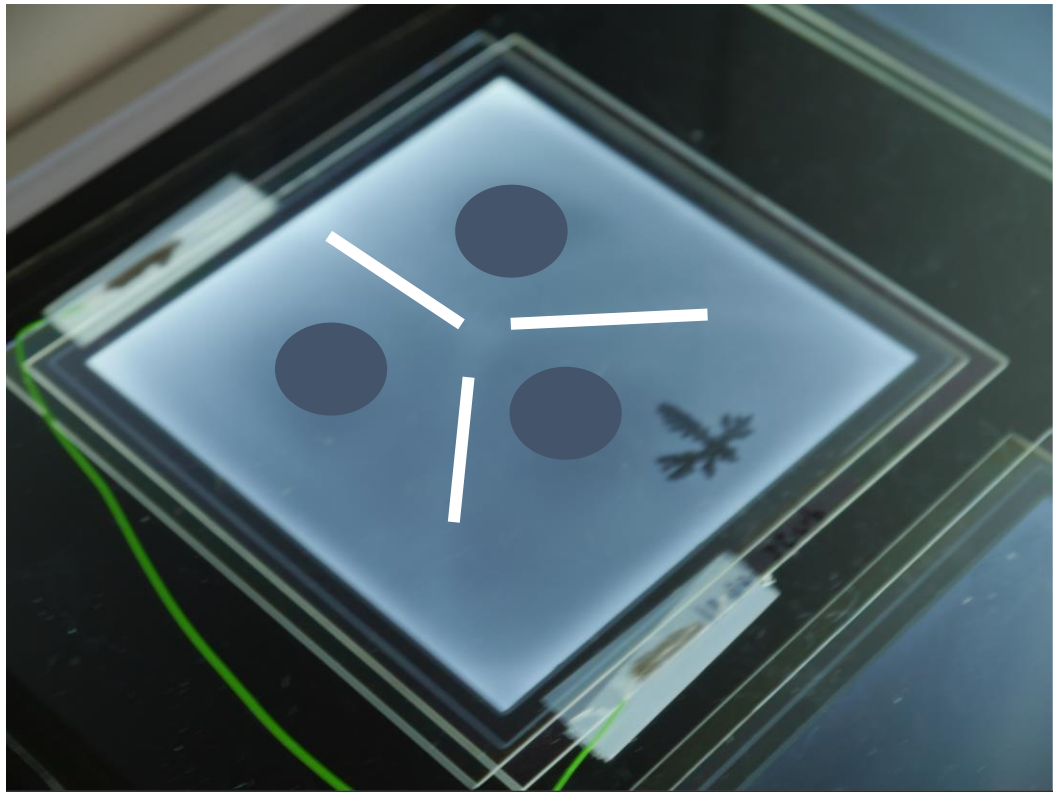

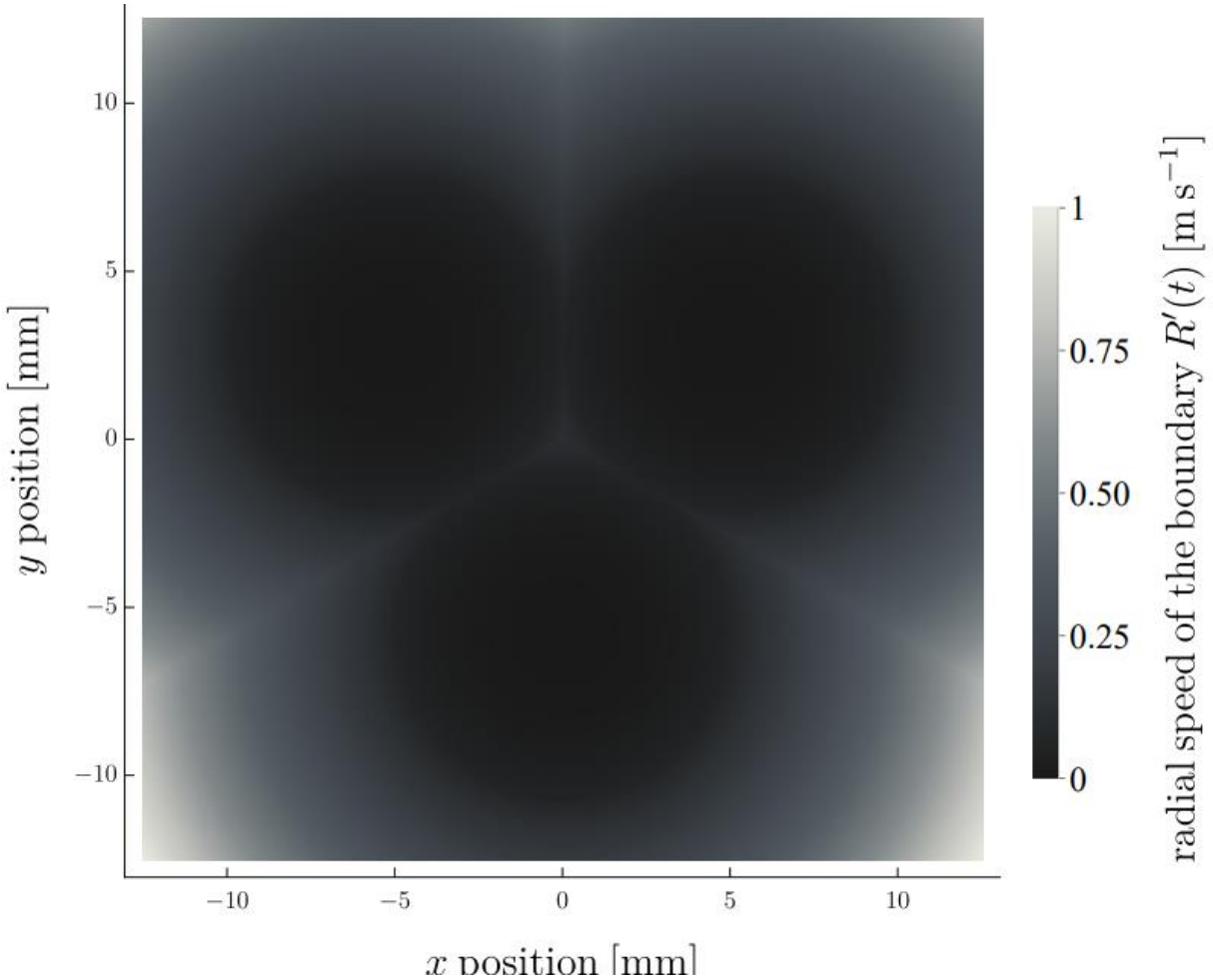

WETTING AND DEWETTING

The ODF method could be improved by controlling the nematic wetting behaviour.

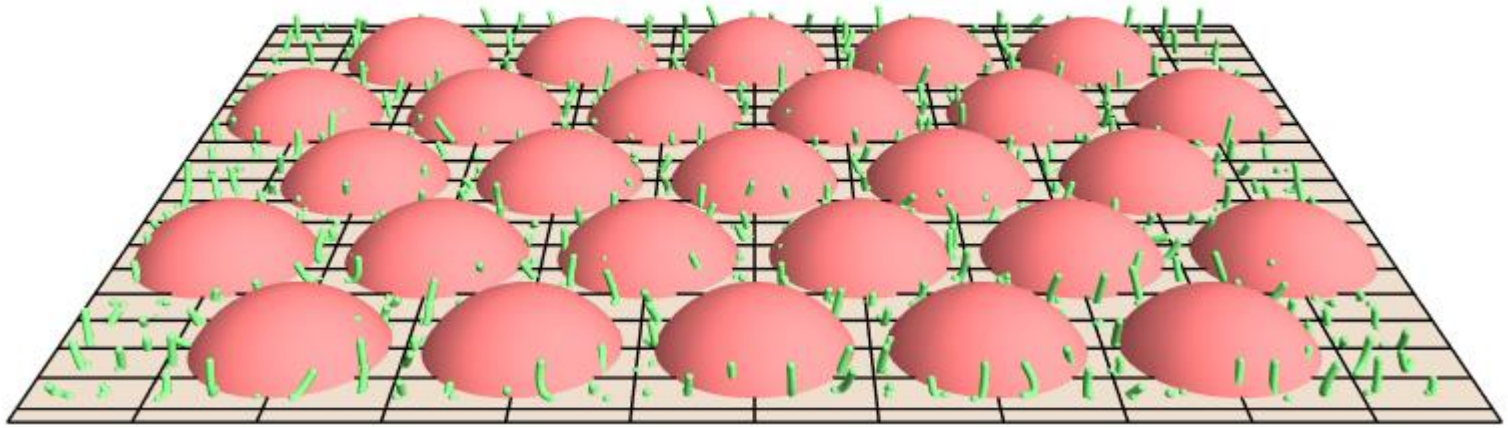

WETTING AND DEWETTING

The ODF method could be improved by controlling the nematic wetting behaviour.

WETTING AND DEWETTING

Simply stated, *wetting* and *dewetting* are the phenomena in which a liquid advances and retreats, respectively, over a substrate. When a finite volume of liquid advances or retreats over a flat horizontal substrate, it will eventually reach an equilibrium state.

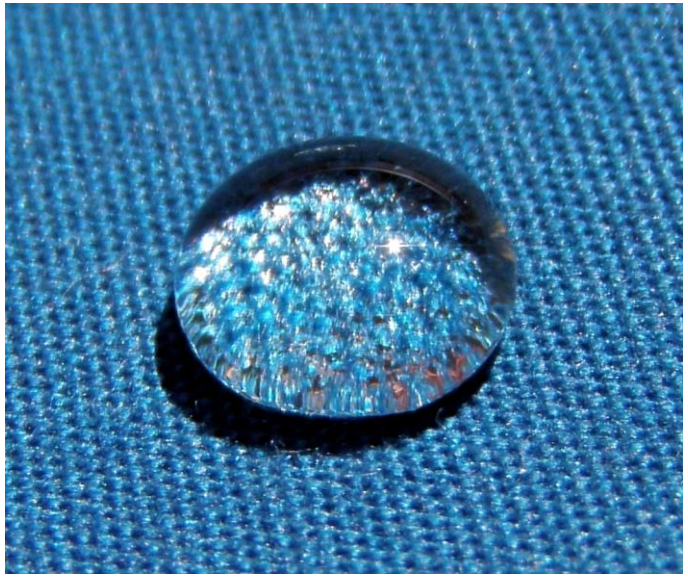

de Gennes et al. *Capillarity and wetting phenomena* (2004).

A NEMATIC RIDGE

To understand this behaviour further, we consider a static ridge of nematic (N) resting on an ideal solid substrate (S) in an atmosphere of passive gas (G).

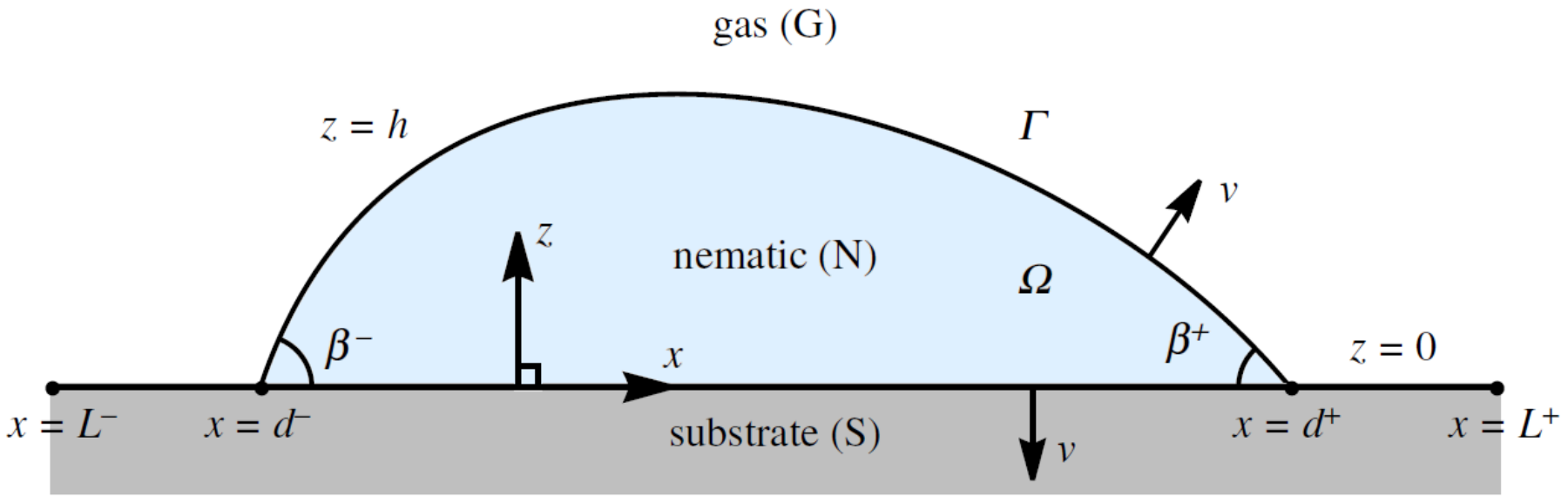

We assume that the director $\boldsymbol{n}$ is confined to the (x, z)-plane, and hence takes the form

$$\boldsymbol{n} = \cos\theta\,\hat{\boldsymbol{x}} + \sin\theta\,\hat{\boldsymbol{z}}.$$

A NEMATIC RIDGE

To understand this behaviour further, we consider a static ridge of nematic (N) resting on an ideal solid substrate (S) in an atmosphere of passive gas (G).

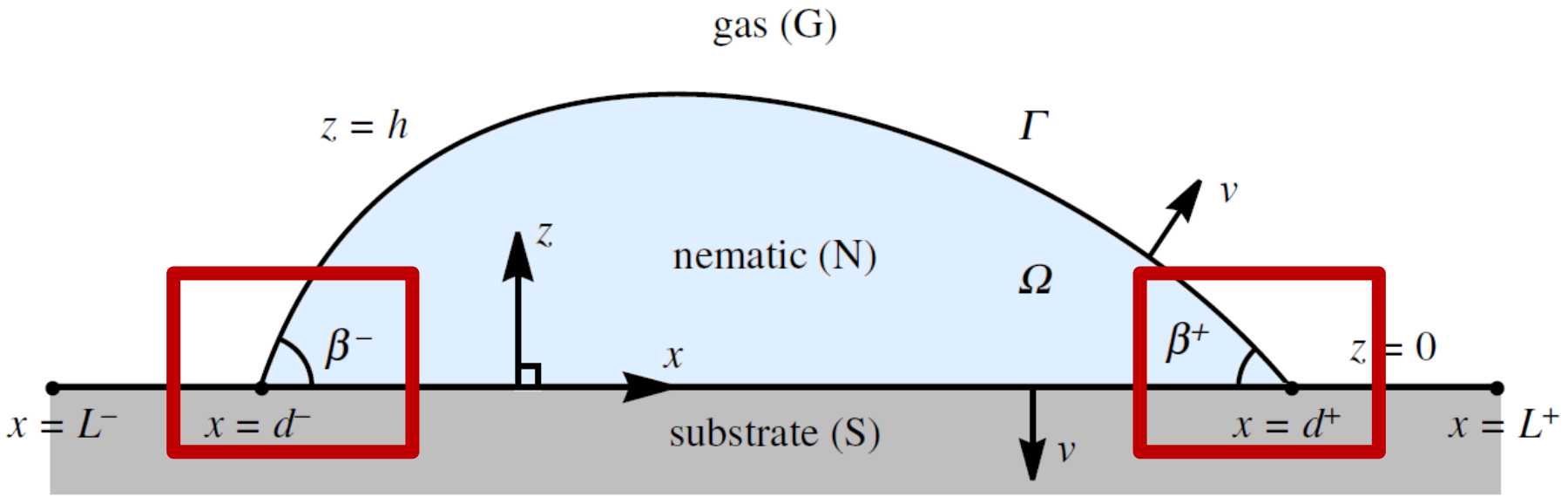

We assume that the director $\boldsymbol{n}$ is confined to the (x, z)-plane, and hence takes the form

$$\boldsymbol{n} = \cos\theta\,\hat{\boldsymbol{x}} + \sin\theta\,\hat{\boldsymbol{z}}.$$

WEAK ANCHORING

The orientational anisotropy of nematics results in an anisotropic component of surface tension that creates an energetic preference for the director to align either normally or tangentially to interfaces; this is known as *weak anchoring*.

We use the standard Rapini-Papoular interfacial energy density to describe the weak anchoring at the interfaces, namely

$$\omega_{GN} = \gamma_{GN} + \frac{C_{GN}}{4}\left(1 - 2(\boldsymbol{\nu}_{GN} \cdot \boldsymbol{n})^2\right)$$

$$\omega_{NS} = \gamma_{NS} + \frac{C_{NS}}{4}\left(1 - 2(\boldsymbol{\nu}_{NS} \cdot \boldsymbol{n})^2\right),$$

where C_{GN} and C_{NS} are the anchoring strength of the GN and NS interfaces, respectively.

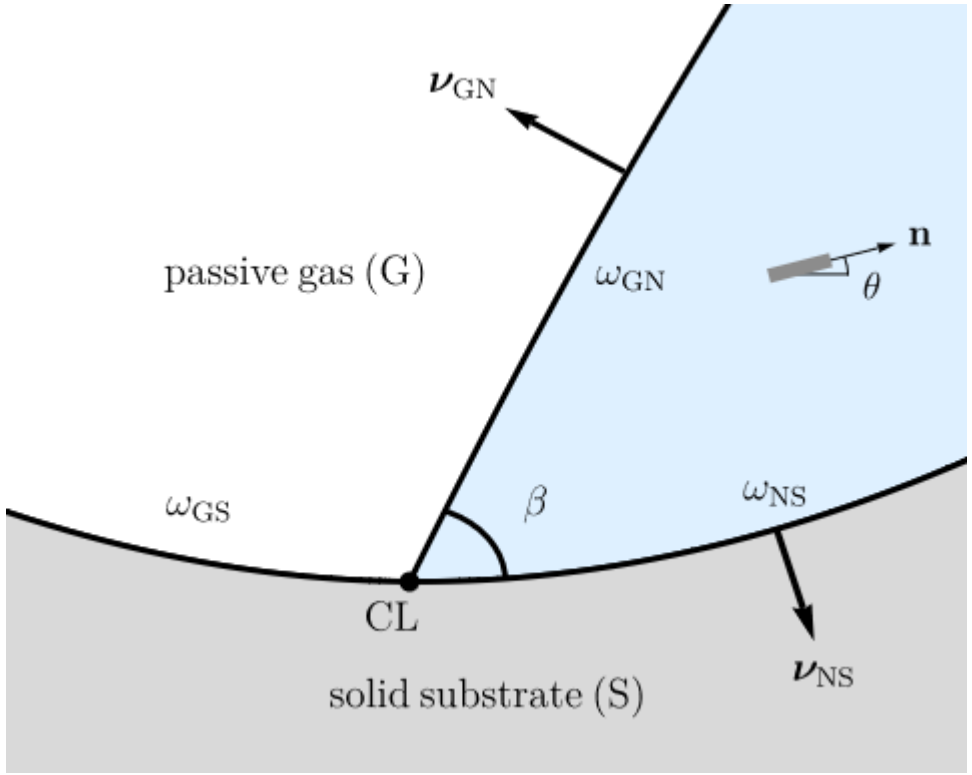

Rapini and Papoular. *J. Phys. Colloquia* **30**:C4-54-C4-56 (1969).

WEAK ANCHORING

The orientational anisotropy of nematics results in an anisotropic component of surface tension that creates an energetic preference for the director to align either normally or tangentially to interfaces; this is known as *weak anchoring*.

We use the standard Rapini-Papoular interfacial energy density to describe the weak anchoring at the interfaces, namely

$$\omega_{GN} = \gamma_{GN} + \frac{C_{GN}}{4}\left(1 - 2(\boldsymbol{v}_{GN} \cdot \boldsymbol{n})^2\right)$$

$$\omega_{NS} = \gamma_{NS} + \frac{C_{NS}}{4}\left(1 - 2(\boldsymbol{v}_{NS} \cdot \boldsymbol{n})^2\right),$$

where C_{GN} and C_{NS} are the anchoring strength of the GN and NS interfaces, respectively.

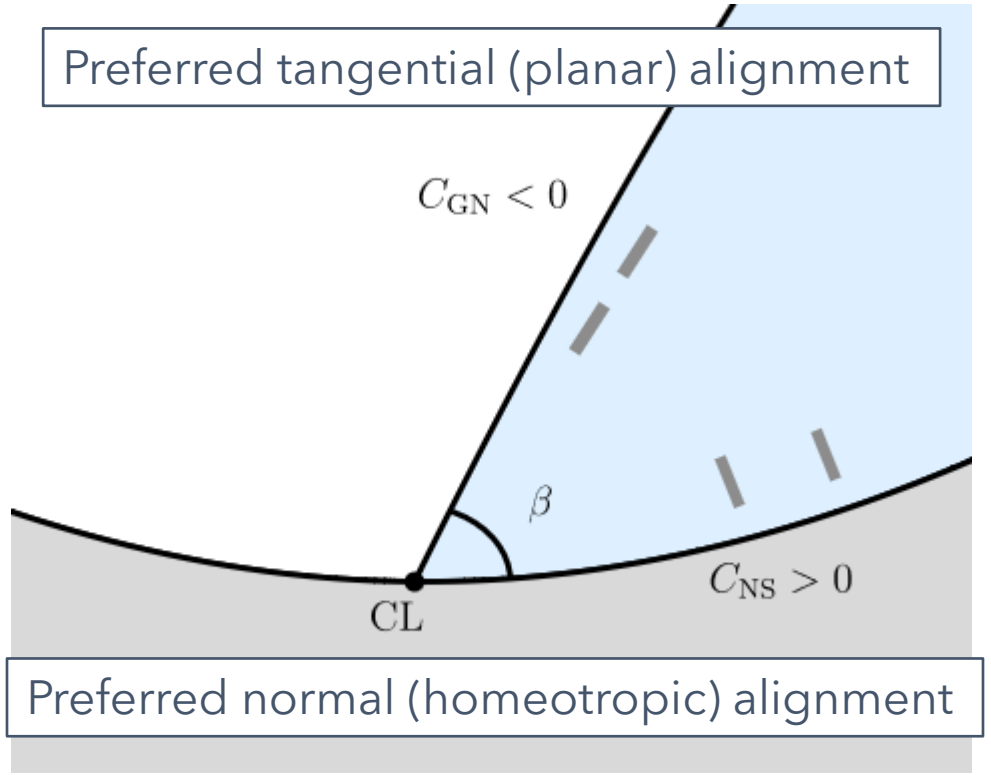

Rapini and Papoular. *J. Phys. Colloquia* **30**:C4-54-C4-56 (1969).

WEAK ANCHORING

The orientational anisotropy of nematics results in an anisotropic component of surface tension that creates an energetic preference for the director to align either normally or tangentially to interfaces; this is known as *weak anchoring*.

We use the standard Rapini-Papoular interfacial energy density to describe the weak anchoring at the interfaces, namely

$$\omega_{GN} = \gamma_{GN} + \frac{C_{GN}}{4}\left(1 - 2(\boldsymbol{v}_{GN} \cdot \boldsymbol{n})^2\right)$$

$$\omega_{NS} = \gamma_{NS} + \frac{C_{NS}}{4}\left(1 - 2(\boldsymbol{v}_{NS} \cdot \boldsymbol{n})^2\right),$$

where C_{GN} and C_{NS} are the anchoring strength of the GN and NS interfaces, respectively.

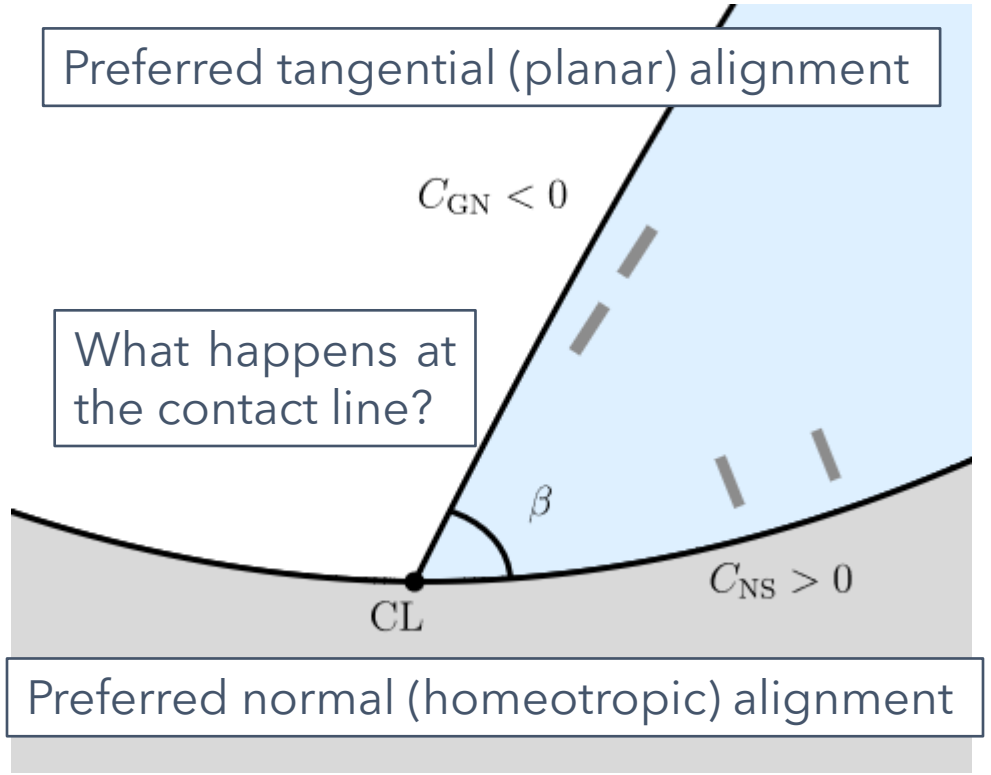

Rapini and Papoular. *J. Phys. Colloquia* **30**:C4-54-C4-56 (1969).

CALCULUS OF VARIATIONS

We define the functional F as the sum of the free energy of the system and a term corresponding to an area constraint, given by

$$\mathcal{C}_{\text{area}} = p_0 \times \left(A - \int_{d^-}^{d^+} \int_0^h \mathrm{d}z\,\mathrm{d}x \right),$$

so that the functional F is given by

$$F = E_{\text{bulk}} + E_{\text{GN}} + E_{\text{NS}} + E_{\text{GS}} + \mathcal{C}_{\text{area}}.$$

We now consider the variation of F with respect to small variations of the variables

$$\theta \to \theta + \delta_\theta, \quad h \to h + \delta_h,$$
$$d^- \to d^- + \delta_{d^-} \quad \text{and} \quad d^+ \to d^+ + \delta_{d^+}.$$

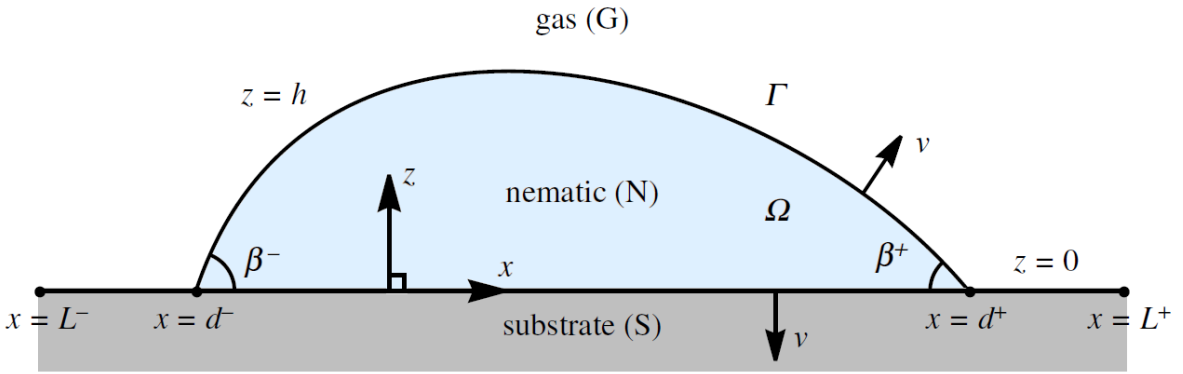

$$E_{\text{bulk}} = \int_{d^-}^{d^+} \int_0^h \left(W_{\text{bulk}}(\theta, \theta_x, \theta_z) + \psi_{\text{g}} \right) \mathrm{d}z\,\mathrm{d}x,$$

$$E_{\text{GN}} = \int_{d^-}^{d^+} \sqrt{1 + h_x^2}\, \left[\omega_{\text{GN}}(\theta, h_x) \right]^{z=h} \mathrm{d}x,$$

$$E_{\text{NS}} = \int_{d^-}^{d^+} \left[\omega_{\text{NS}}(\theta) \right]^{z=0} \mathrm{d}x$$

$$E_{\text{GS}} = \int_{L^-}^{d^-} \left[\omega_{\text{GS}} \right]^{z=0} \mathrm{d}x + \int_{d^+}^{L^+} \left[\omega_{\text{GS}} \right]^{z=0} \mathrm{d}x.$$

NEMATIC YOUNG EQUATIONS

Using the Calculus of Variations, we derive the nematic Young equation at each contact line:

$$\gamma_{GS} - \gamma_{NS} - \gamma_{GN}\cos\beta^{-} = \frac{C_{NS}}{4}\cos 2\theta + \frac{C_{GN}}{4}[\cos 2(\theta - \beta^{-})\cos\beta^{-} - 2\sin 2(\theta - \beta^{-})\sin\beta^{-}]$$

$$\text{at } x = d^{-}$$

and

$$\gamma_{GS} - \gamma_{NS} - \gamma_{GN}\cos\beta^{+} = \frac{C_{NS}}{4}\cos 2\theta + \frac{C_{GN}}{4}[\cos 2(\theta + \beta^{+})\cos\beta^{+} - 2\sin 2(\theta + \beta^{+})\sin\beta^{+}]$$

$$\text{at } x = d^{+}.$$

NEMATIC YOUNG EQUATIONS

Using the Calculus of Variations, we derive the nematic Young equation at each contact line:

$$\underbrace{\gamma_{GS} - \gamma_{NS} - \gamma_{GN}\cos\beta^{-}}_{\text{at } x = d^{-}} = \frac{C_{NS}}{4}\cos 2\theta + \frac{C_{GN}}{4}\left[\cos 2(\theta - \beta^{-})\cos\beta^{-} - 2\sin 2(\theta - \beta^{-})\sin\beta^{-}\right]$$

and

$$\underbrace{\gamma_{GS} - \gamma_{NS} - \gamma_{GN}\cos\beta^{+}}_{\text{at } x = d^{+}.} = \frac{C_{NS}}{4}\cos 2\theta + \frac{C_{GN}}{4}\left[\cos 2(\theta + \beta^{+})\cos\beta^{+} - 2\sin 2(\theta + \beta^{+})\sin\beta^{+}\right]$$

NEMATIC YOUNG EQUATIONS

Using the Calculus of Variations, we derive the nematic Young equation at each contact line:

$$\underbrace{\gamma_{GS} - \gamma_{NS} - \gamma_{GN}\cos\beta^{-}}_{\text{at } x = d^{-}} = \frac{C_{NS}}{4}\cos 2\theta + \frac{C_{GN}}{4}\left[\cos 2(\theta - \beta^{-})\cos\beta^{-} - 2\sin 2(\theta - \beta^{-})\sin\beta^{-}\right]$$

and

$$\underbrace{\gamma_{GS} - \gamma_{NS} - \gamma_{GN}\cos\beta^{+}}_{\text{at } x = d^{+}.} = \frac{C_{NS}}{4}\cos 2\theta + \frac{C_{GN}}{4}\left[\cos 2(\theta + \beta^{+})\cos\beta^{+} - 2\sin 2(\theta + \beta^{+})\sin\beta^{+}\right]$$

WHAT HAPPENS AT THE CONTACT LINE?

To analyse the nematic Young equations, we need to understand the director angle at the contact line.

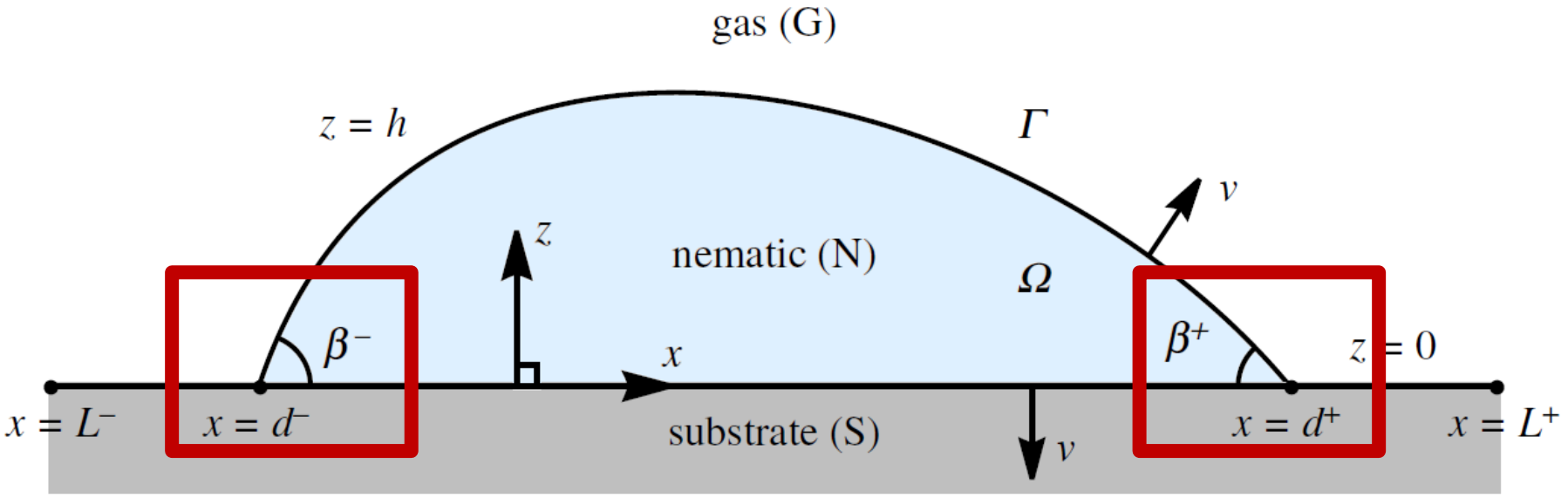

WHAT HAPPENS AT THE CONTACT LINE?

To analyse the nematic Young equations, we need to understand the director angle at the contact line.

To gain a further understanding of the behaviour at the contact line we consider a thin ridge.

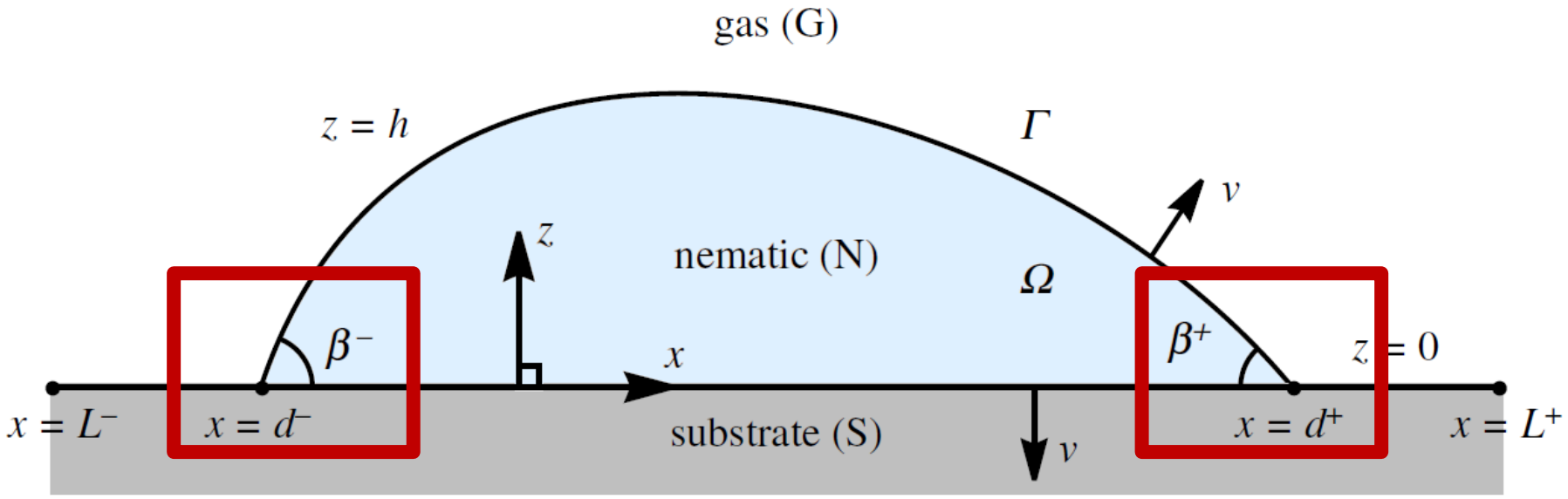

WHAT HAPPENS FOR A THIN RIDGE?

A thin-film limit of the governing equations for a nematic ridge yield the following leading-order equations:

Director angle solution:

$$\theta(x,z) = \left(\theta_{\mathrm{GN}}(x) - \theta_{\mathrm{NS}}(x)\right)\frac{z}{h(x)} + \theta_{\mathrm{NS}}(x)$$

Interface conditions:

$$K\left(\theta_{\mathrm{GN}} - \theta_{\mathrm{NS}}\right) + C_{\mathrm{NS}} h \sin\theta_{\mathrm{NS}} \cos\theta_{\mathrm{NS}} = 0$$

$$K\left(\theta_{\mathrm{GN}} - \theta_{\mathrm{NS}}\right) - C_{\mathrm{GN}} h \sin\theta_{\mathrm{GN}} \cos\theta_{\mathrm{GN}} = 0$$

$$p_0 + h_{xx} + \frac{K}{2}\left(\frac{\theta_{\mathrm{GN}} - \theta_{\mathrm{NS}}}{h}\right)^2 = 0$$

Constraints:

$$h = 0 \quad \text{at} \quad x = \pm d$$

$$1 = \int_{-d}^{d} h \, \mathrm{d}x$$

Pinned CLs:
d – is prescribed

Unpinned CLs:
d – is unknown:

$$\mp h_x = \beta = \left(2 + \frac{1}{2}(C_{\mathrm{NS}} + C_{\mathrm{GN}})\cos 2\theta\right)^{1/2} \quad \text{at} \quad x = \pm d$$

WHAT HAPPENS FOR A THIN RIDGE?

Solutions show anchoring breaking occurring at the contact lines.

Pinned CLs:

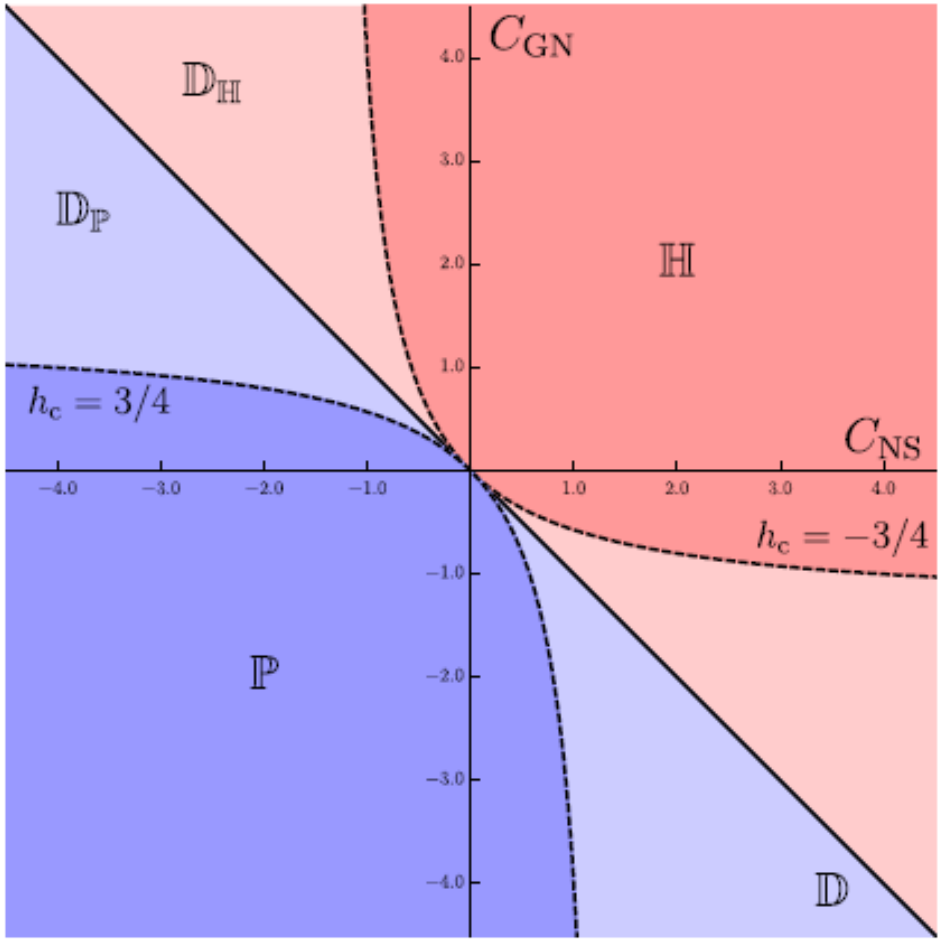

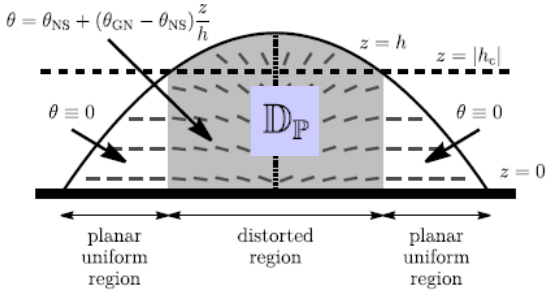

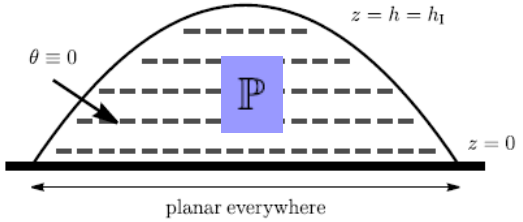

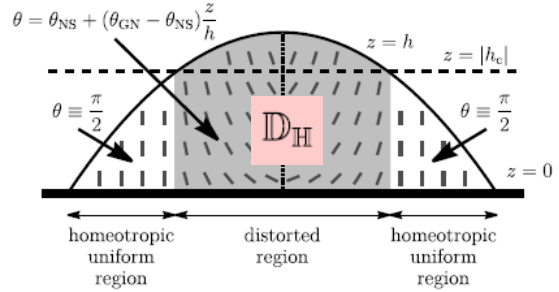

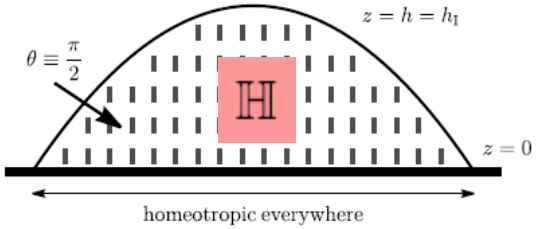

WHAT HAPPENS FOR A THIN RIDGE?

Solutions show anchoring breaking occurring at the contact lines.

Pinned CLs:

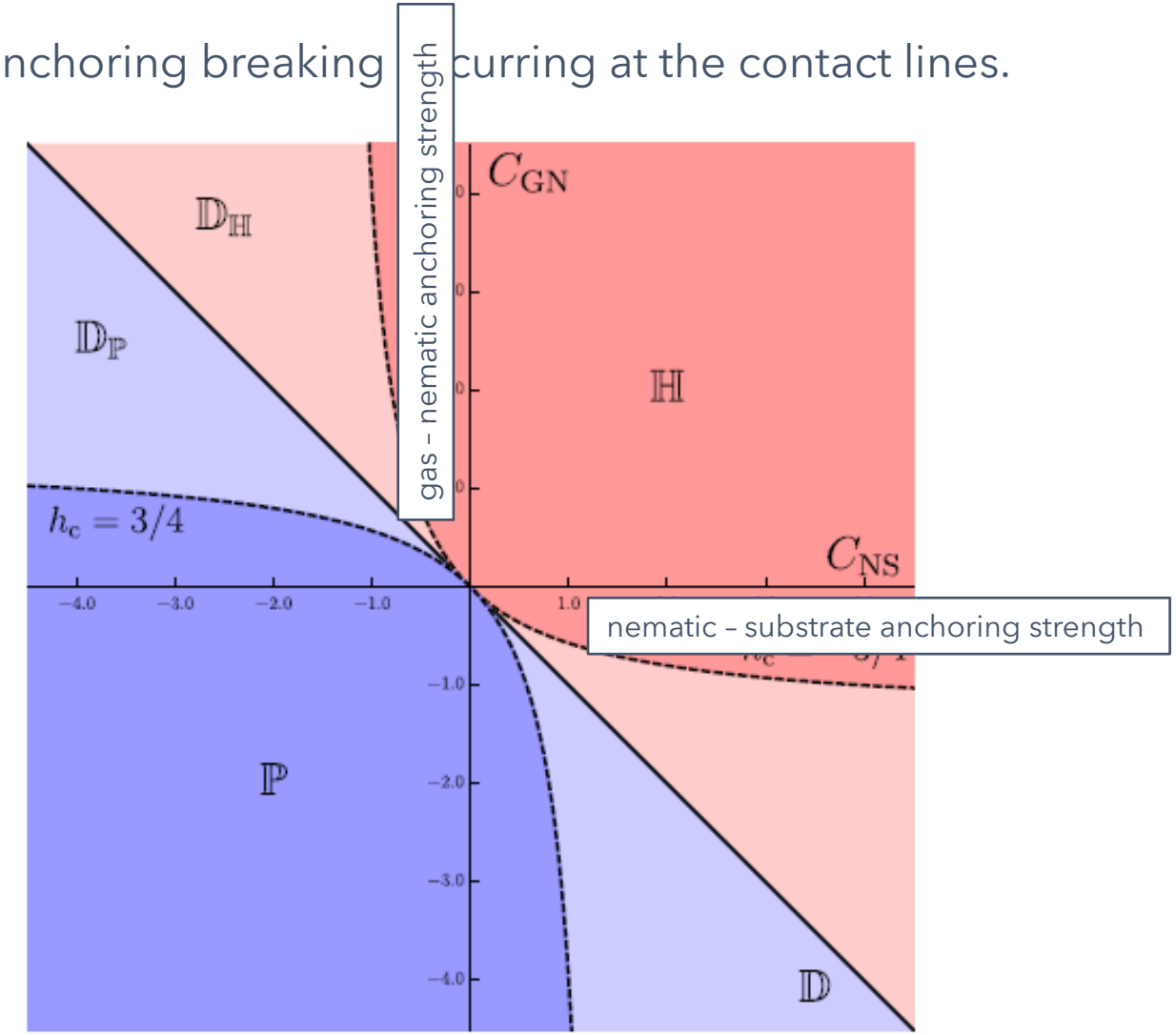

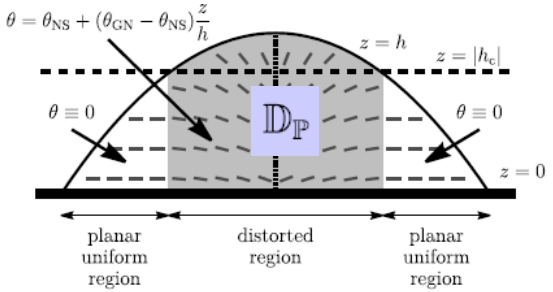

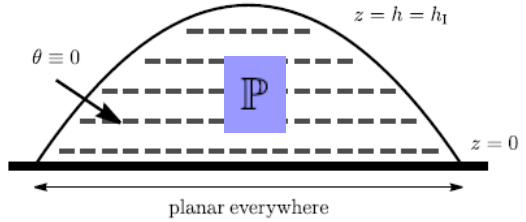

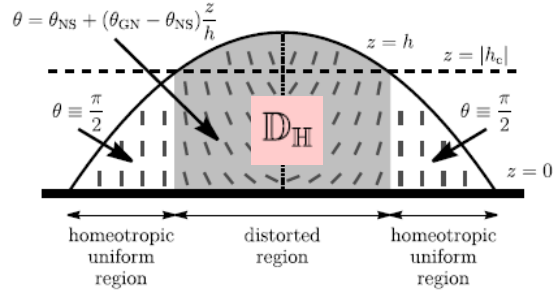

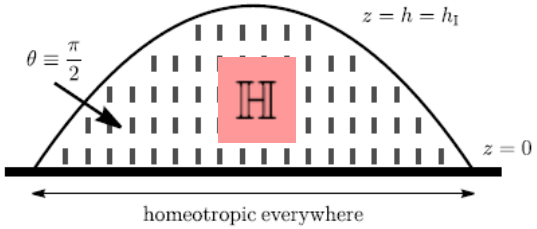

WHAT HAPPENS FOR A THIN RIDGE?

Solutions show anchoring breaking occurring at the contact lines.

Pinned CLs:

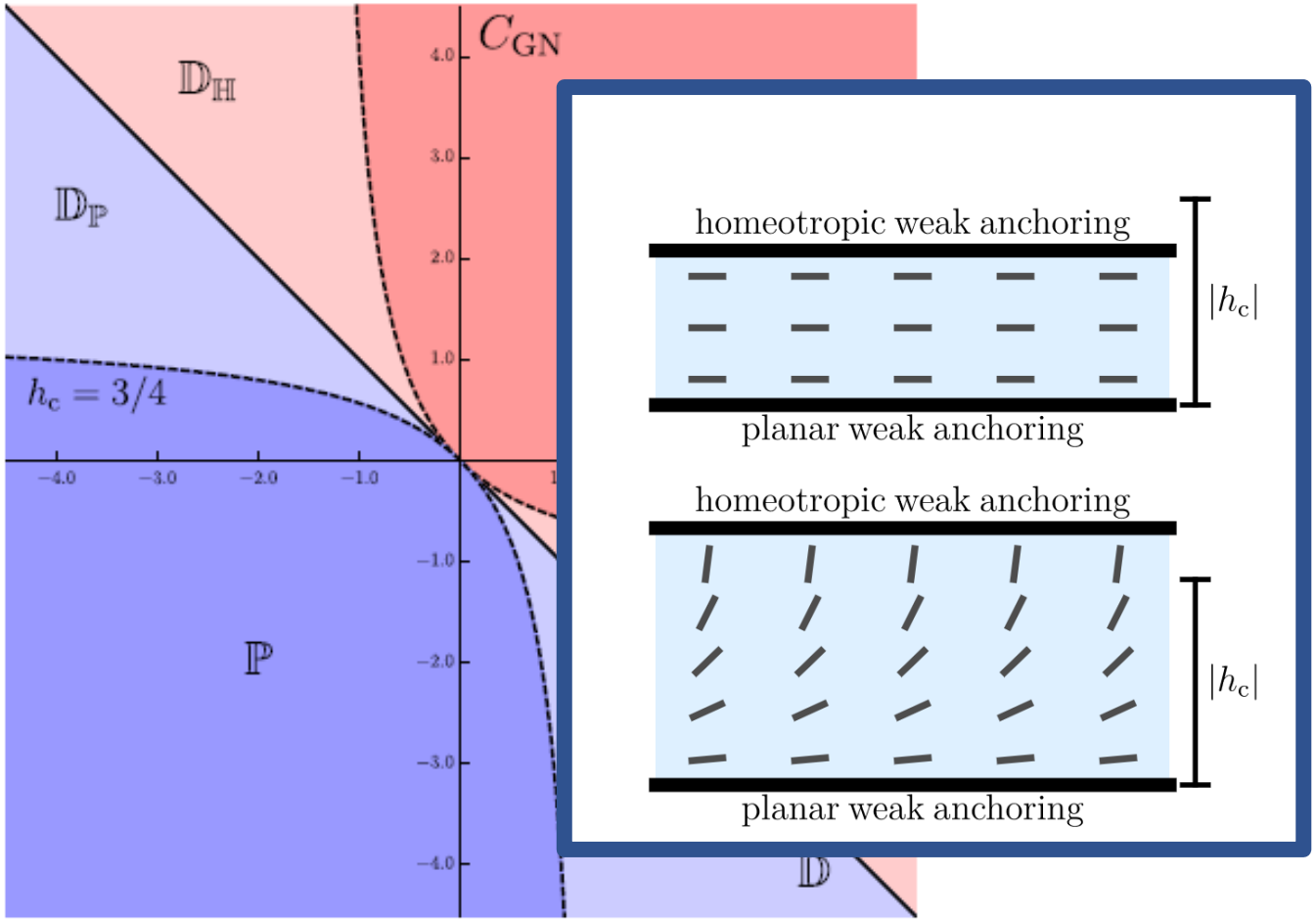

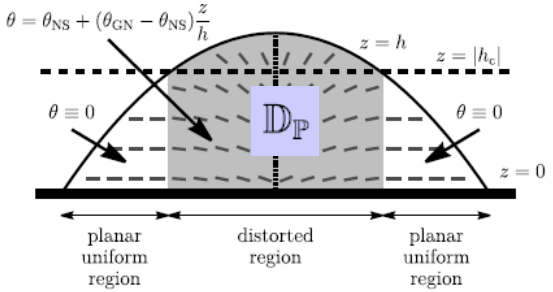

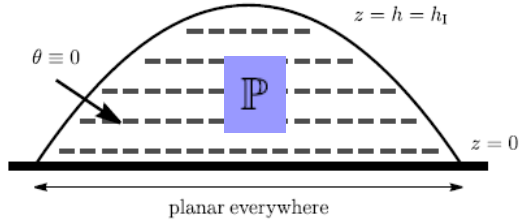

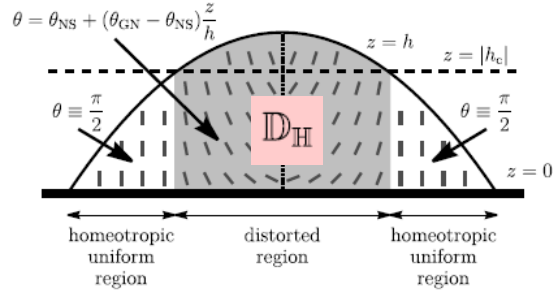

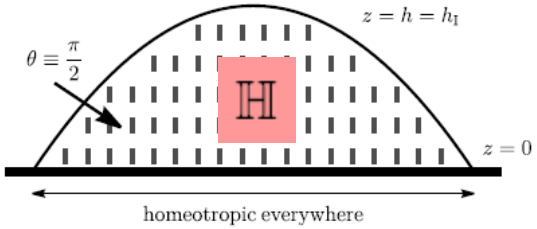

WHAT HAPPENS FOR A THIN RIDGE?

Solutions show anchoring breaking occurring at the contact lines.

Unpinned CLs:

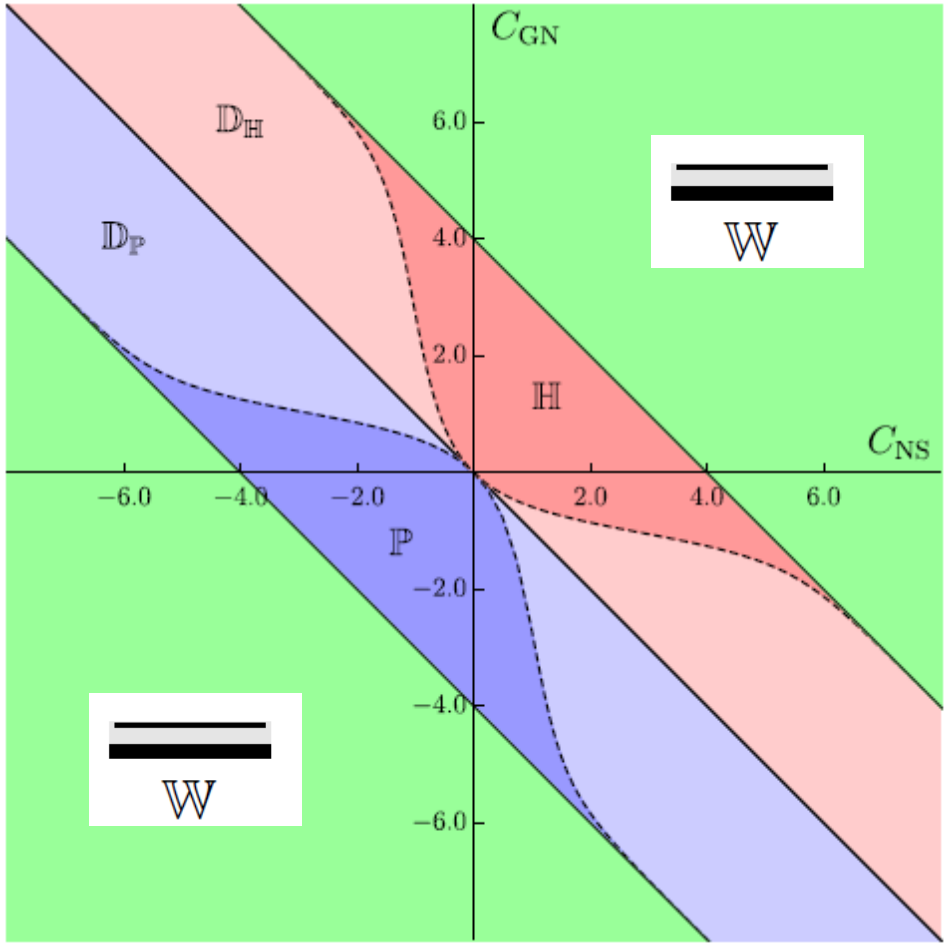

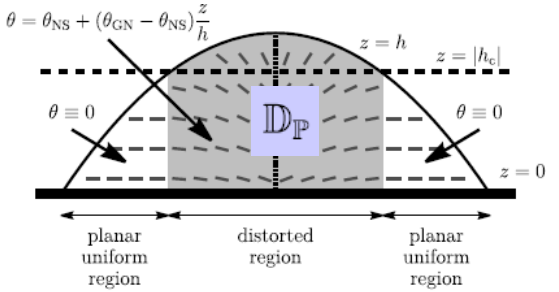

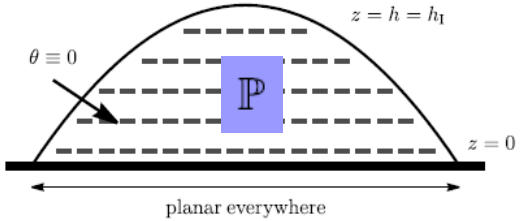

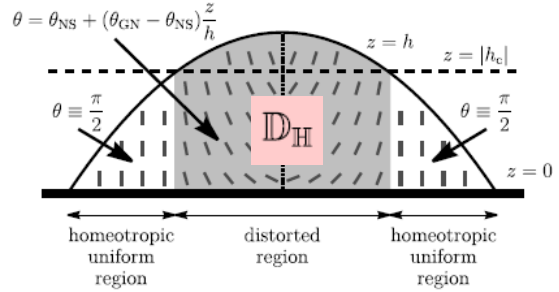

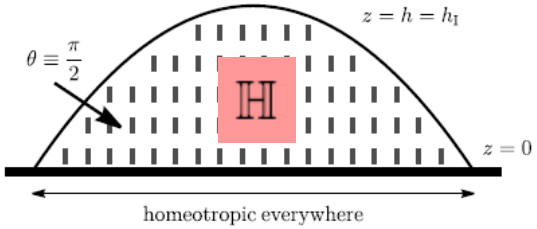

WHAT HAPPENS FOR A THIN RIDGE?

A thin-film limit of the governing equations for a nematic ridge yield the follow leading order equations:

Pinned CLs:

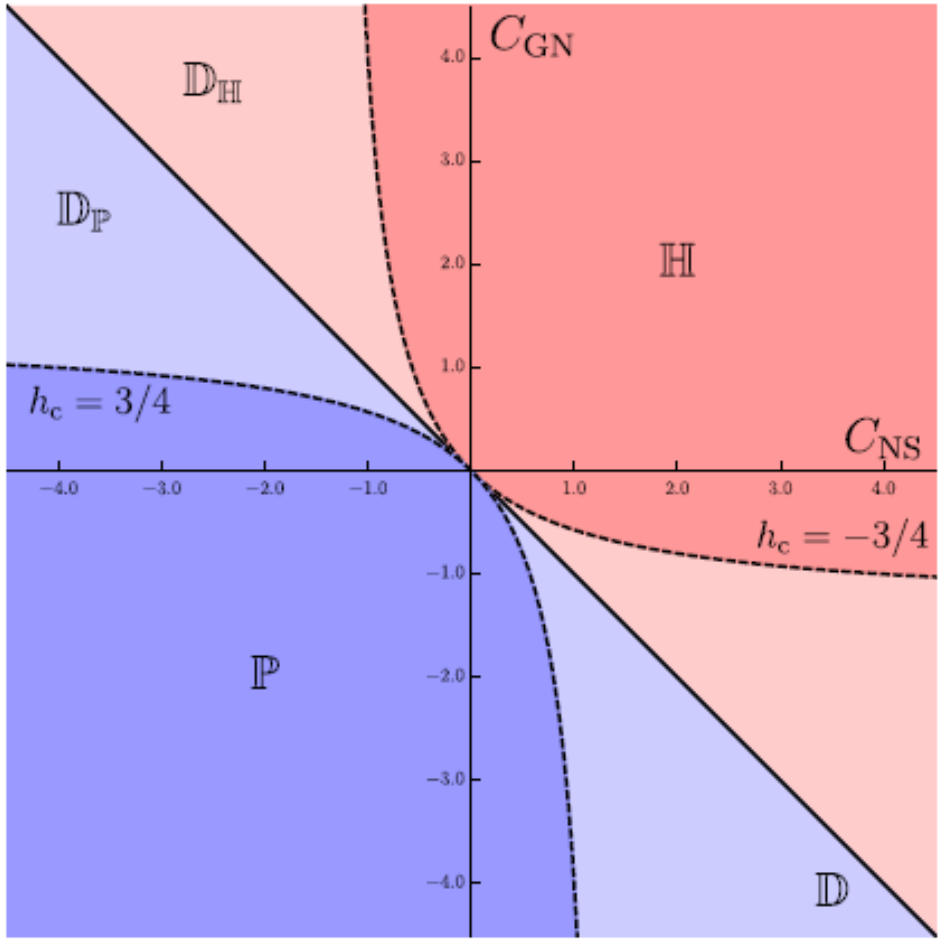

Unpinned CLs:

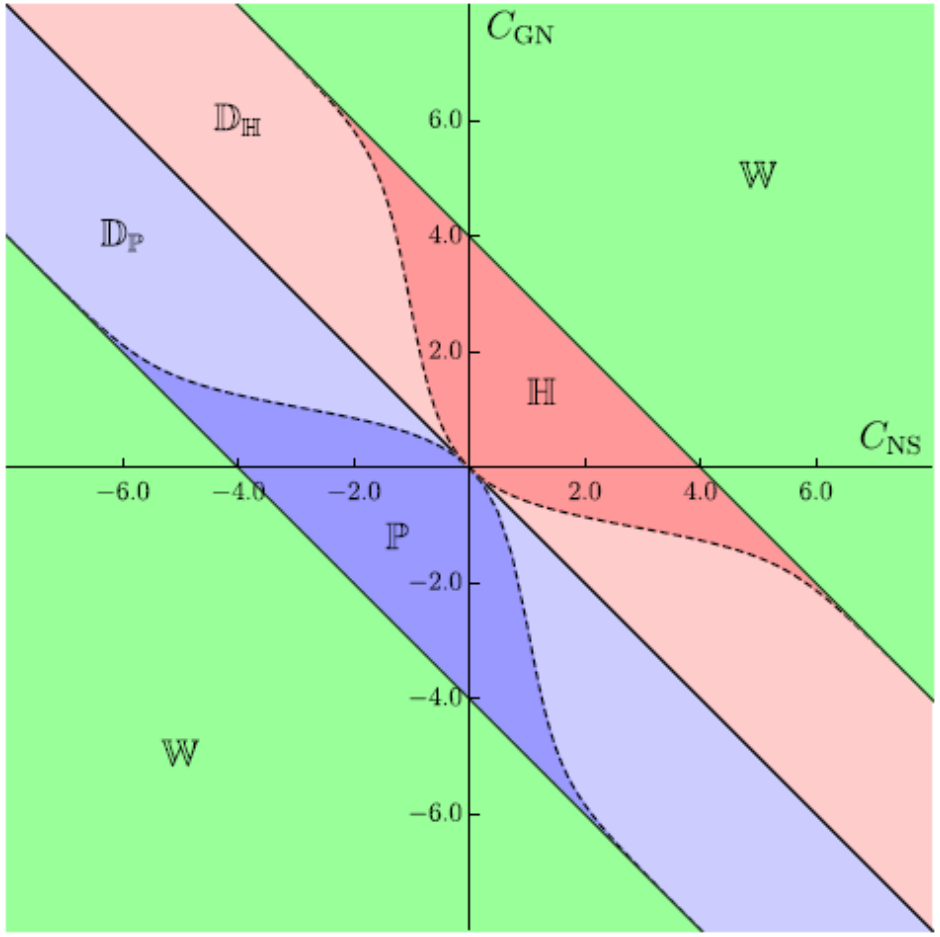

WHAT HAPPENS IN A REAL SYSTEM?

A comparison between the experimental values of and the theoretical predictions for the effective refractive index of a thin pinned ridge [1] has been carried out.

WHAT HAPPENS IN A REAL SYSTEM?

A comparison between the experimental values of and the theoretical predictions for the effective refractive index of a thin pinned ridge [1] has been carried out.

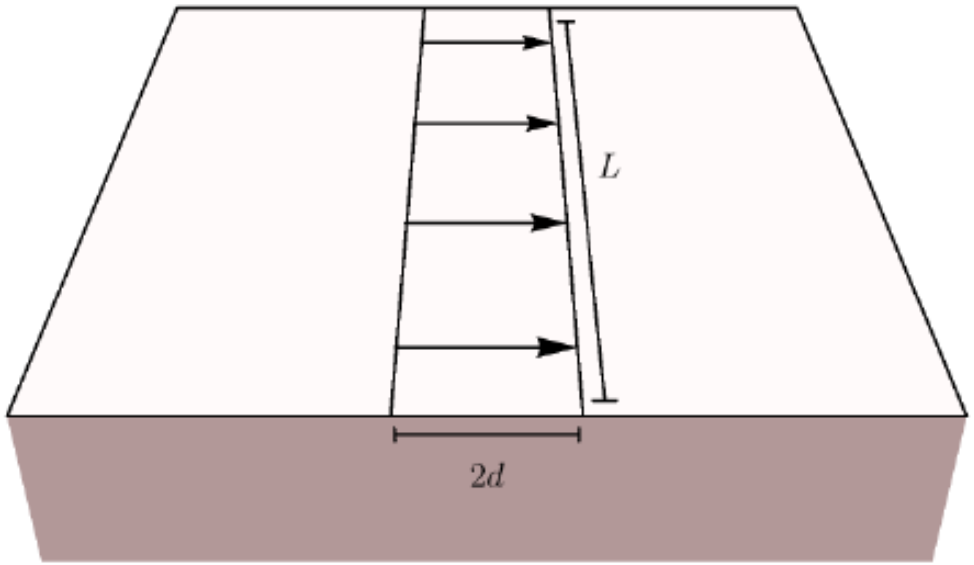

WHAT HAPPENS IN A REAL SYSTEM?

A comparison between the experimental values of and the theoretical predictions for the effective refractive index of a thin pinned ridge [1] has been carried out.

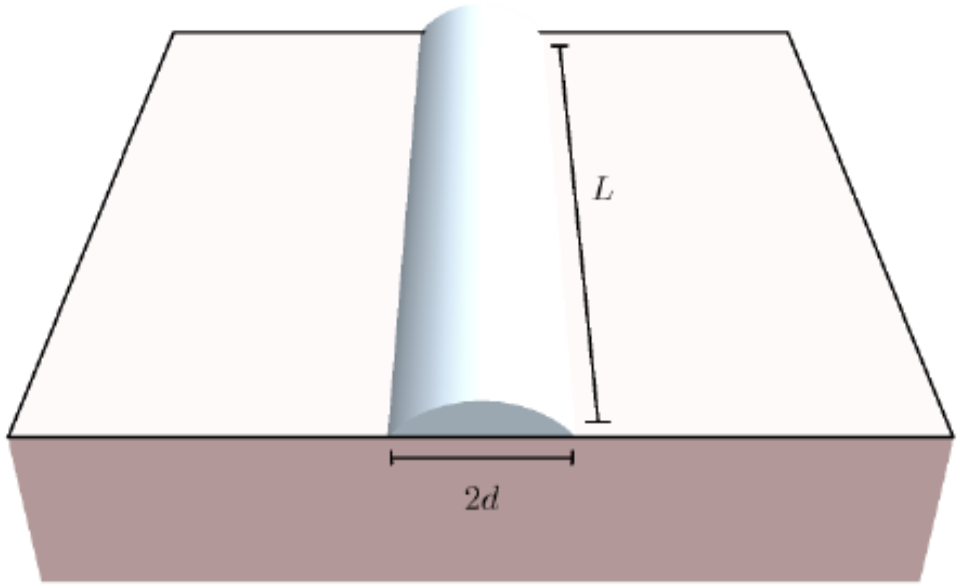

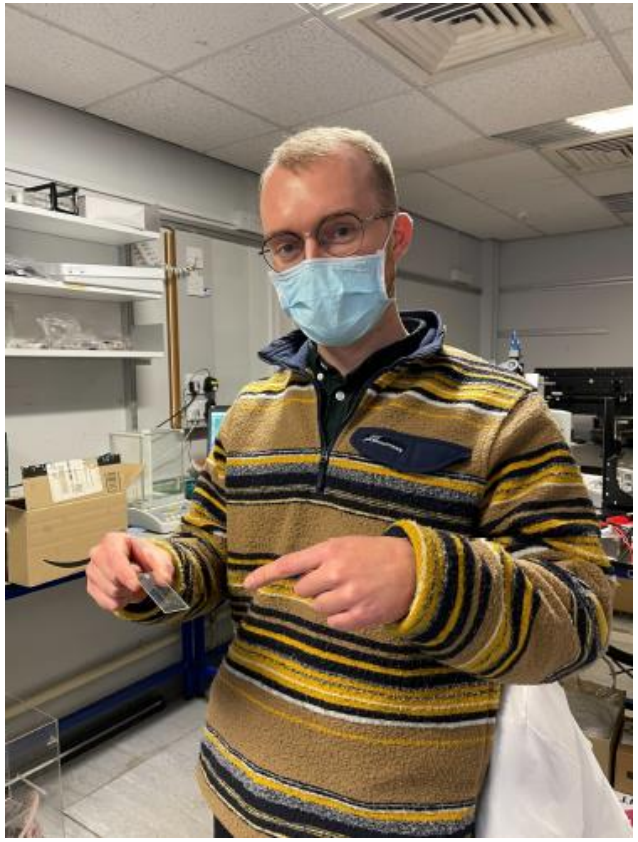

[1] Cousins et al. Submitted to *Phys. Rev. E*, 2022

Nottingham Trent University

WHAT HAPPENS IN A REAL SYSTEM?

A comparison between the experimental values of and the theoretical predictions for the effective refractive index of a thin pinned ridge [1] has been carried out.

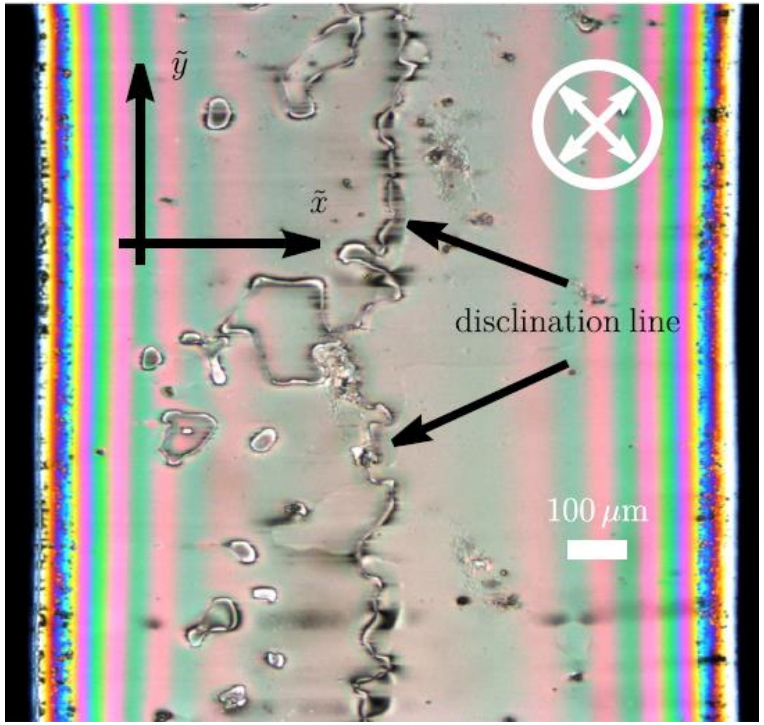

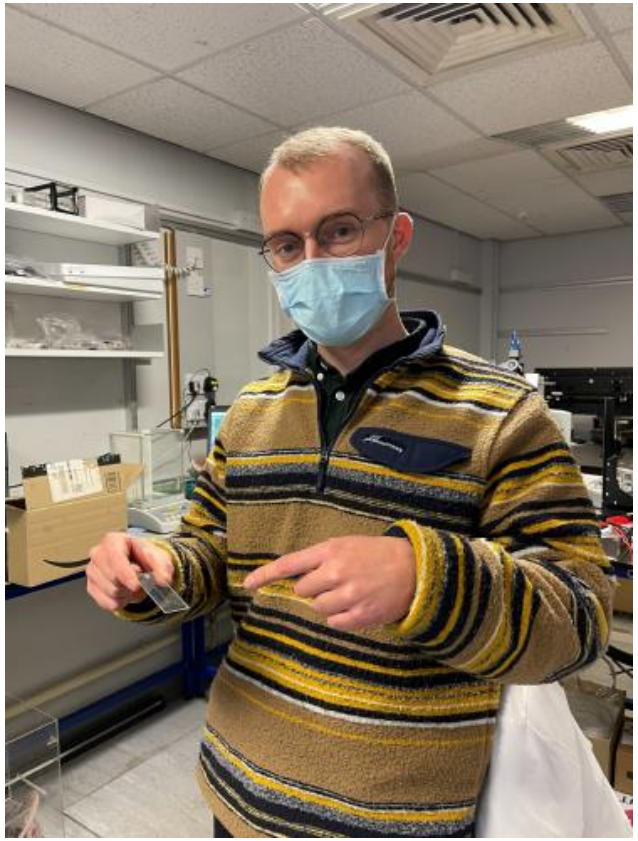

WHAT HAPPENS IN A REAL SYSTEM?

A comparison between the experimental values of and the theoretical predictions for the effective refractive index of a thin pinned ridge is shown below [1].

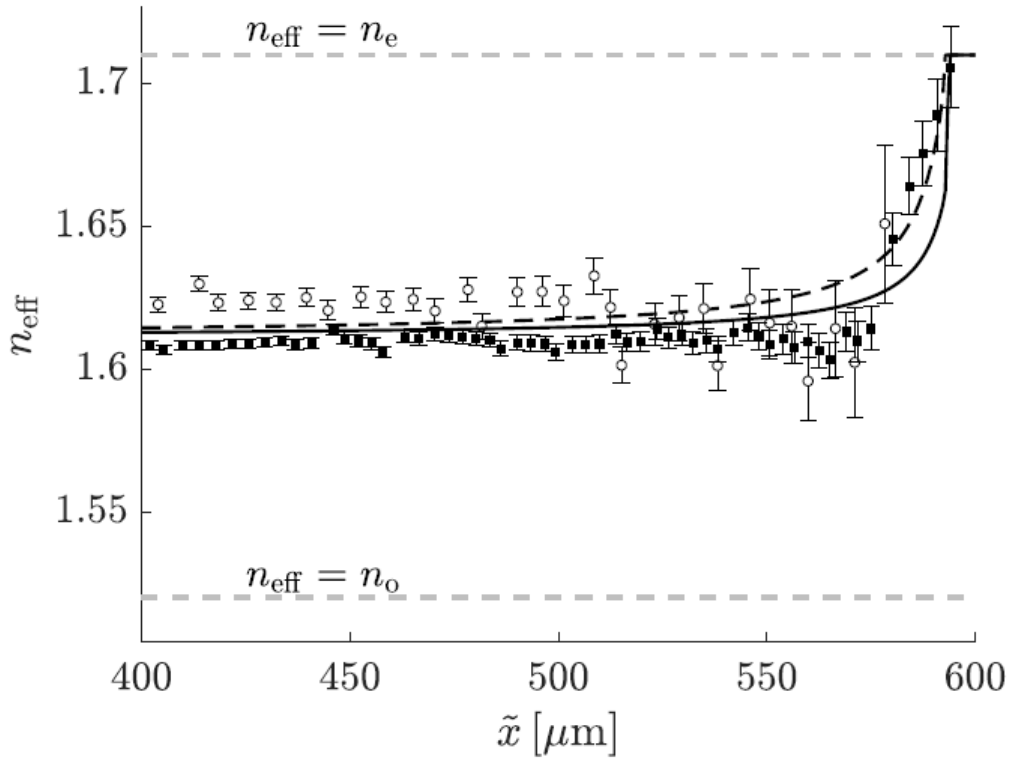

WHAT HAPPENS IN A REAL SYSTEM?

A comparison between the experimental values of and the theoretical predictions for the effective refractive index of a thin pinned ridge is shown below [1].

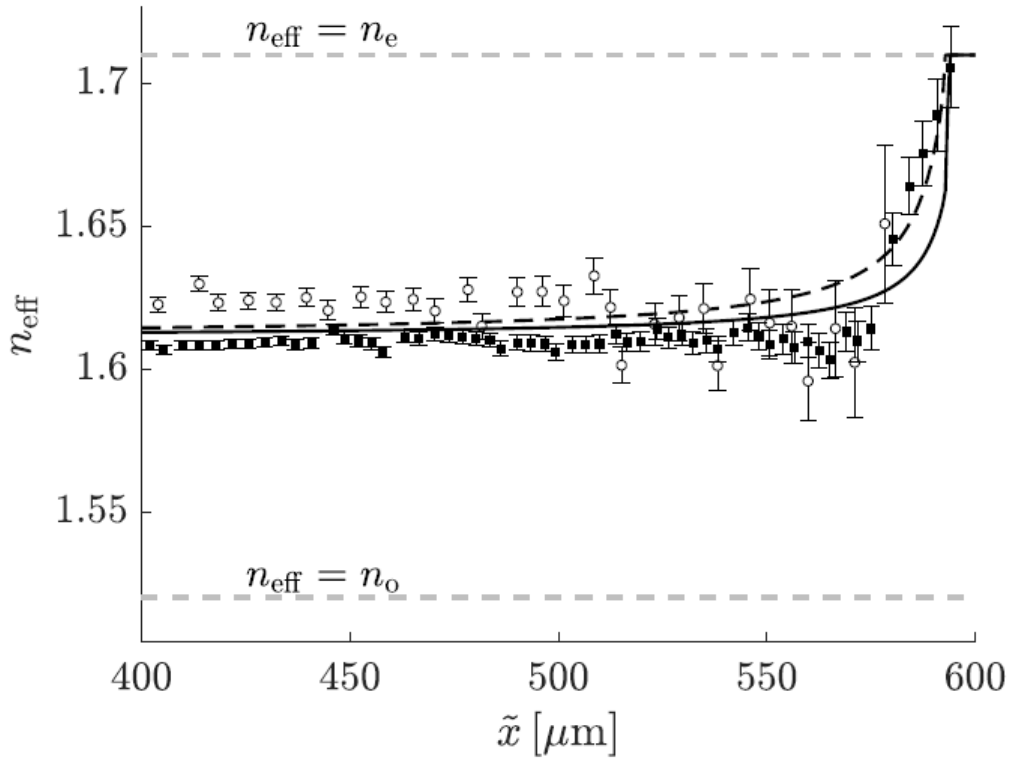

- Both theory and experiment indicate that **anchoring breaking** occurs at the CLs.

- Comparison between the thin-film theory and experiments can be used to determine the free surface anchoring strength.

WHAT HAPPENS AT THE CONTACT LINE?

Both theory and experiment indicate that **anchoring breaking** occurs at the CLs.

WHAT HAPPENS AT THE CONTACT LINE?

Both theory and experiment indicate that **anchoring breaking** occurs at the CLs.

If we assume that the nematic-substrate (NS) interface has the highest anchoring strength, anchoring breaking leads to either $\theta = \pi/2$ or $\theta = 0$.

In this case, the nematic Young equation reduces to:

$$S_N + 1 - \cos\beta = -\Delta_{GN}\cos\beta(\cos^2\beta - 1)$$

Compare this to the isotropic Young equation:

$$S_I + 1 - \cos\beta = 0$$

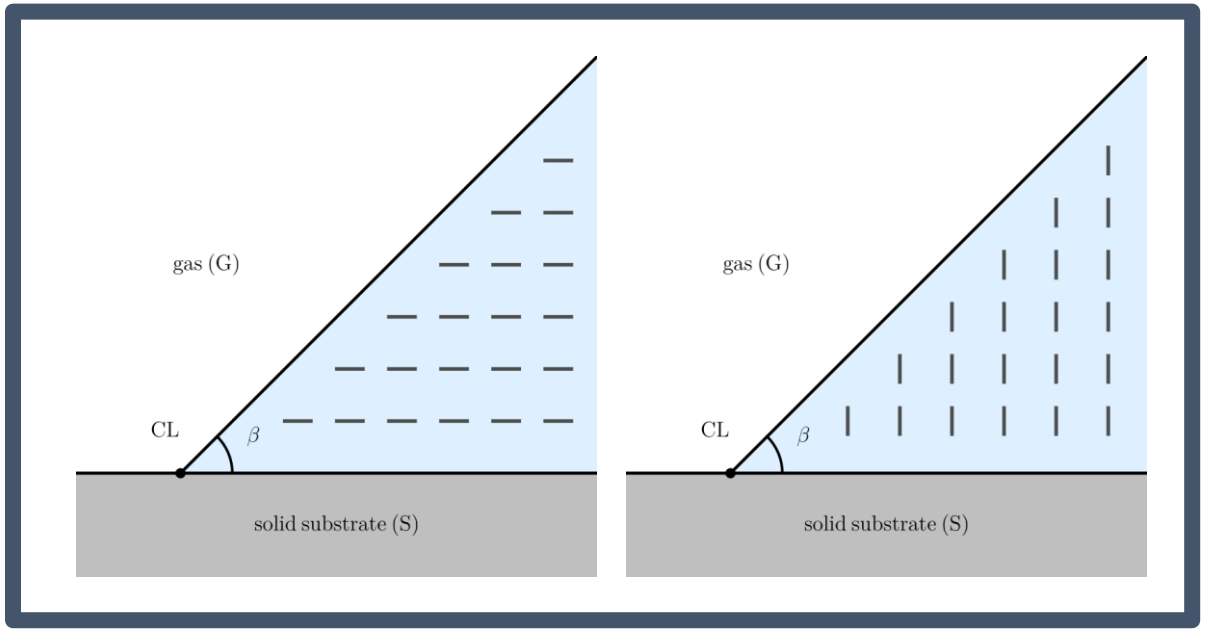

WHAT HAPPENS AT THE CONTACT LINE?

Both theory and experiment indicate that **anchoring breaking** occurs at the CLs.

If we assume that the nemat
interface has the highest an
anchoring breaking leads t
0.

In this case, the nematic You
reduces to:

$$S_N + 1 - \cos\beta = -\Delta_{GN}$$

Compare this to the isotrop

$$S_I + 1 - \cos$$

there may be **defects** (disclination lines in this two-dimensional case) at one or both of the contact lines

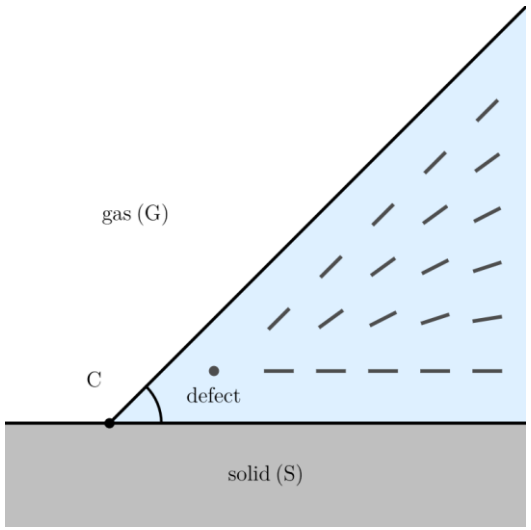

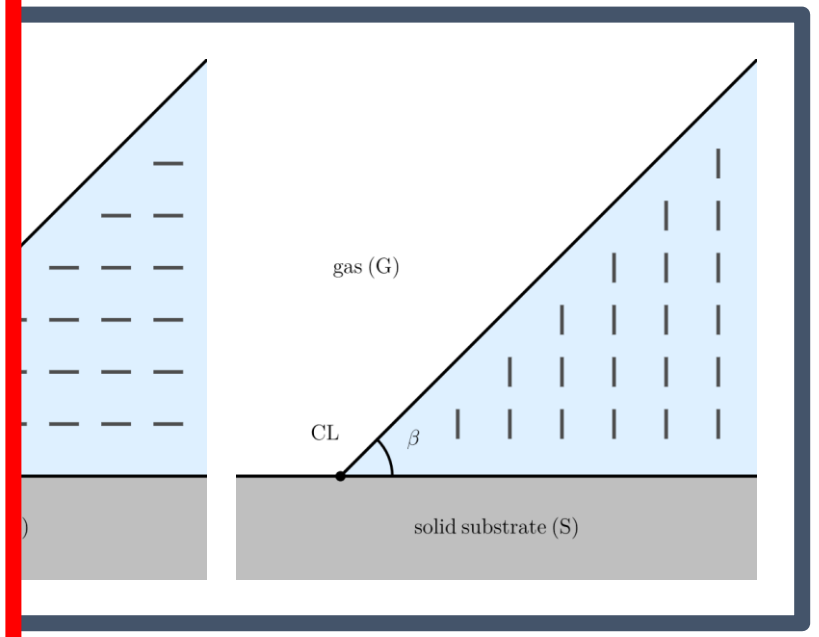

NEMATIC YOUNG EQUATIONS

The nematic Young equations give rise to continuous transitions analogous to those that occur in the classical case of an isotropic liquid, a variety of discontinuous transitions, and contact-angle hysteresis.

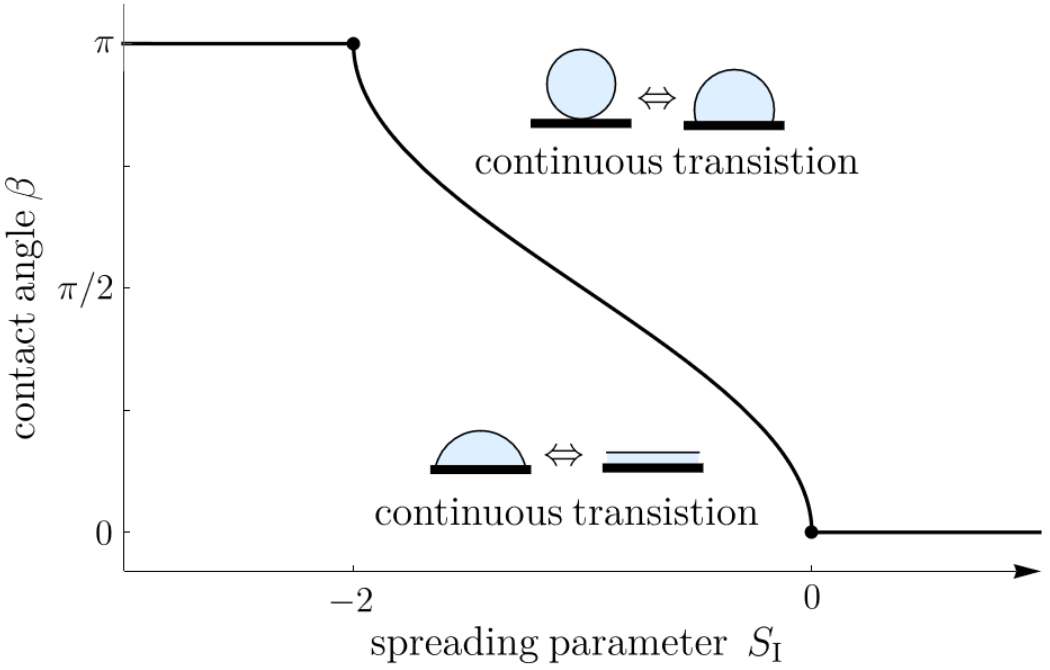

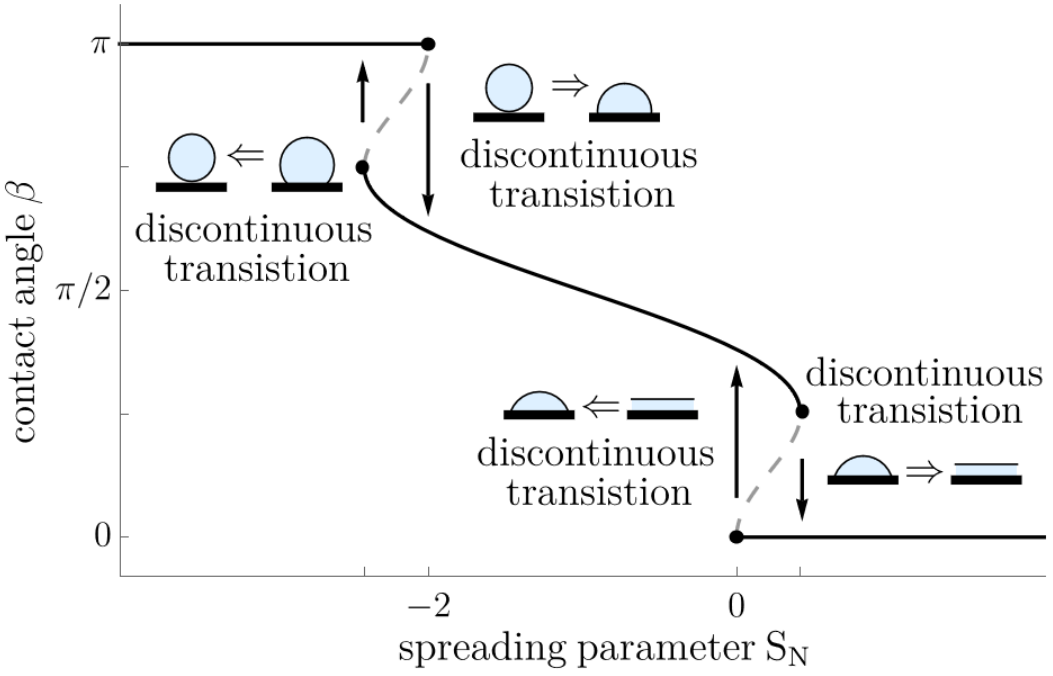

Classical isotropic system

$$S_I + 1 - \cos\beta = 0$$

Nematic system

$$S_N + 1 - \cos\beta = -\Delta_{GN}\cos\beta(\cos^2\beta - 1)$$

CONCLUSIONS

Both theory and experiment indicate that **anchoring breaking** occurs at the CLs. Comparison between the thin-film theory and experiments can be used to determine the free surface anchoring strength.

It was shown that the nematic Young equations in the case of NS-dominant anchoring give rise to

- continuous transitions analogous to those that occur in the classical case of an isotropic liquid,
- a variety of discontinuous transitions,
- contact-angle hysteresis,
- regions of parameter space in which there exist multiple partial wetting states.

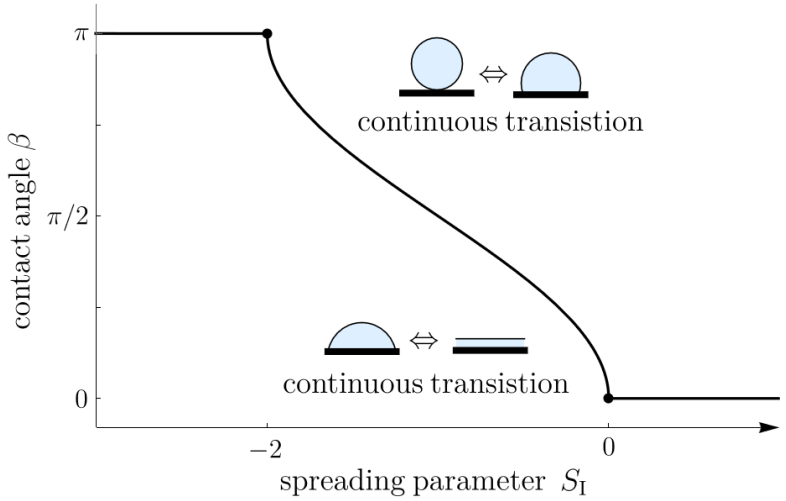

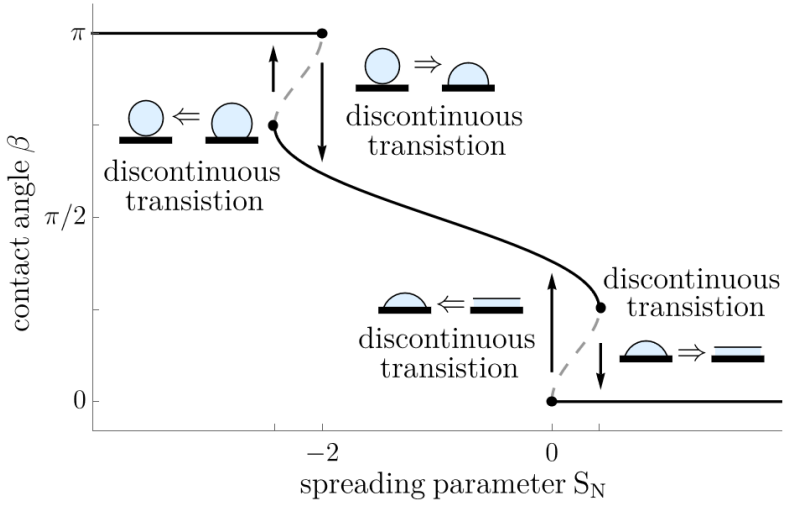

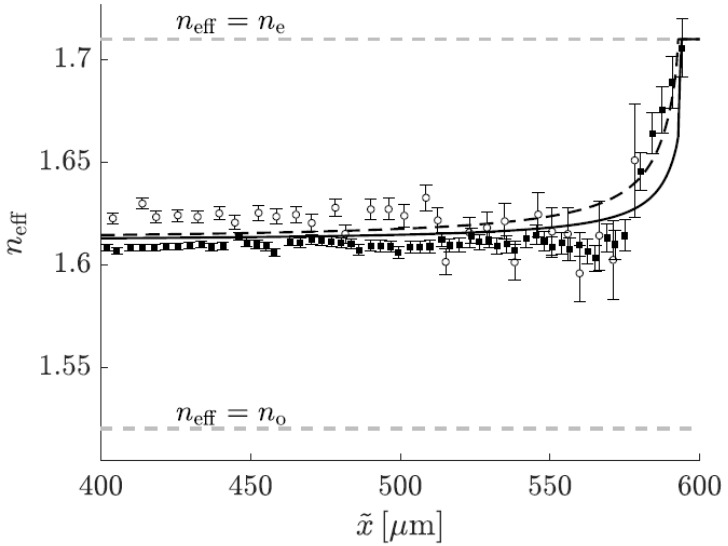

FLOWING RIDGES: RIVULETS

A rivulet is a narrow stream of liquid located on a solid surface

Rivulets of water on a windowpane

RIVULETS

A rivulet is a narrow stream of liquid located on a solid surface

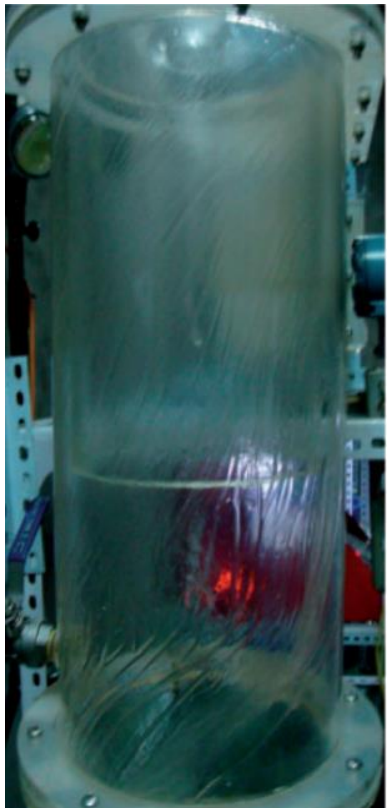

Oil films inside aeroengines [1]

De-icing fluid on an aircraft [2]

Rivulets of rainwater on stay cables [3]

[1] L. Wang, J Process Mechanical Engineering, **231**(1): 14-25, 2017.
[2] https://www.flightradar24.com/blog/ready-for-winter-a-look-at-aircraft-deicing/
[3] S. Jeong et al., *Mathematical Problems in Engineering*, 4138279, 2019

CONTROLLING A NEMATIC RIVULET

Can we use the anisotropic dielectric and viscous properties of nematics to create a rivulet with a controllable viscosity?

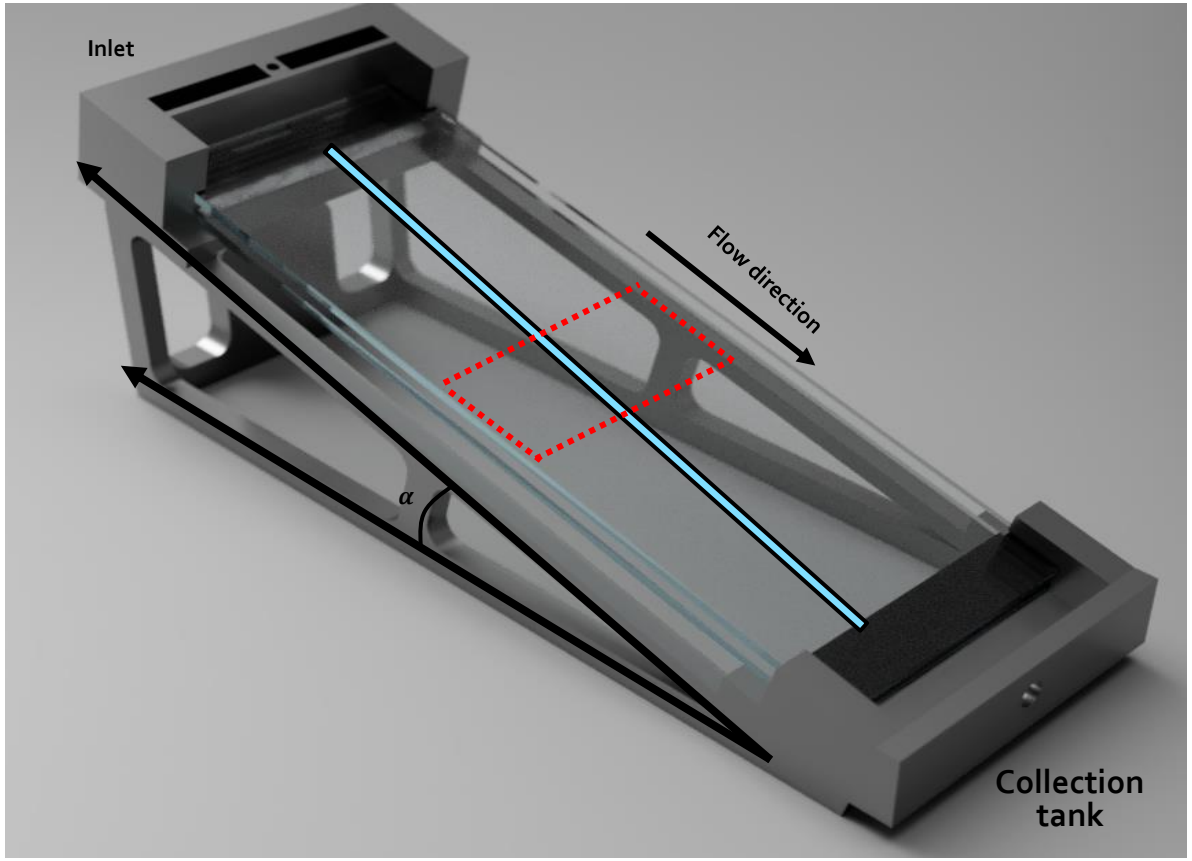

We use a pinned nematic rivulet with a prescribed flux Q positioned between two parallel electrodes.

- controlling the applied electric field can change the average orientation of the nematic molecules.
- this creates a controllable viscosity for the rivulet.
- the change in viscosity induced by the field will change the height and velocity of the rivulet.

CONTROLLING A NEMATIC RIVULET

Can we use the anisotropic dielectric and viscous properties of nematics to create a rivulet with a controllable viscosity?

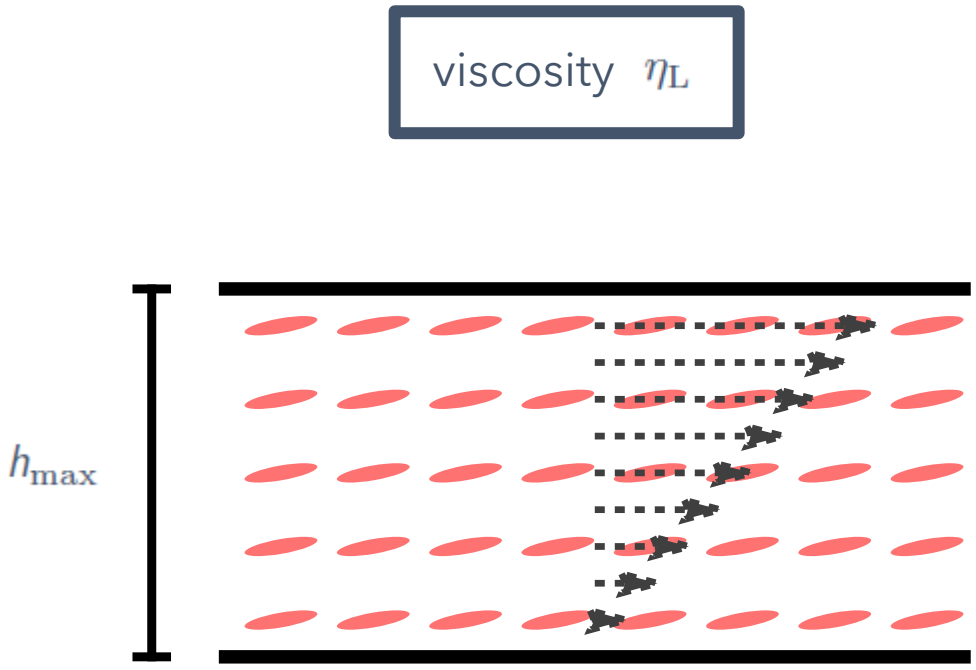

nematic rivulet – **field off**

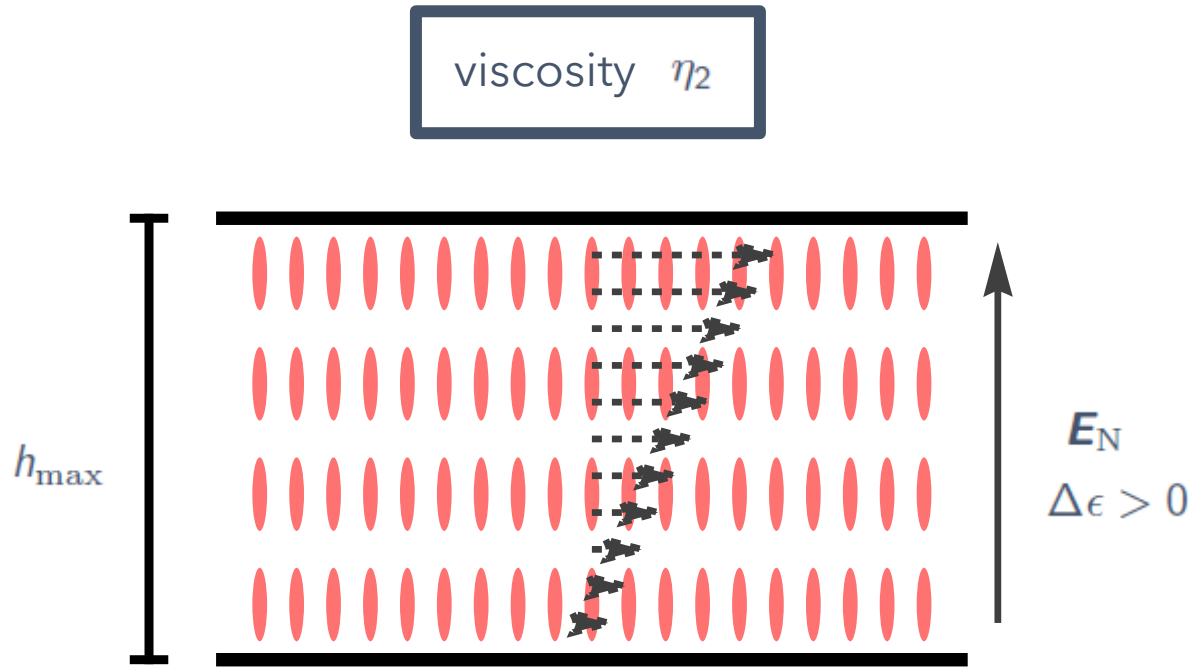

nematic rivulet – **field on**

EXPERIMENTS

Nottingham Trent University

Our collaborators at Nottingham Trent University have brought this idea into reality:

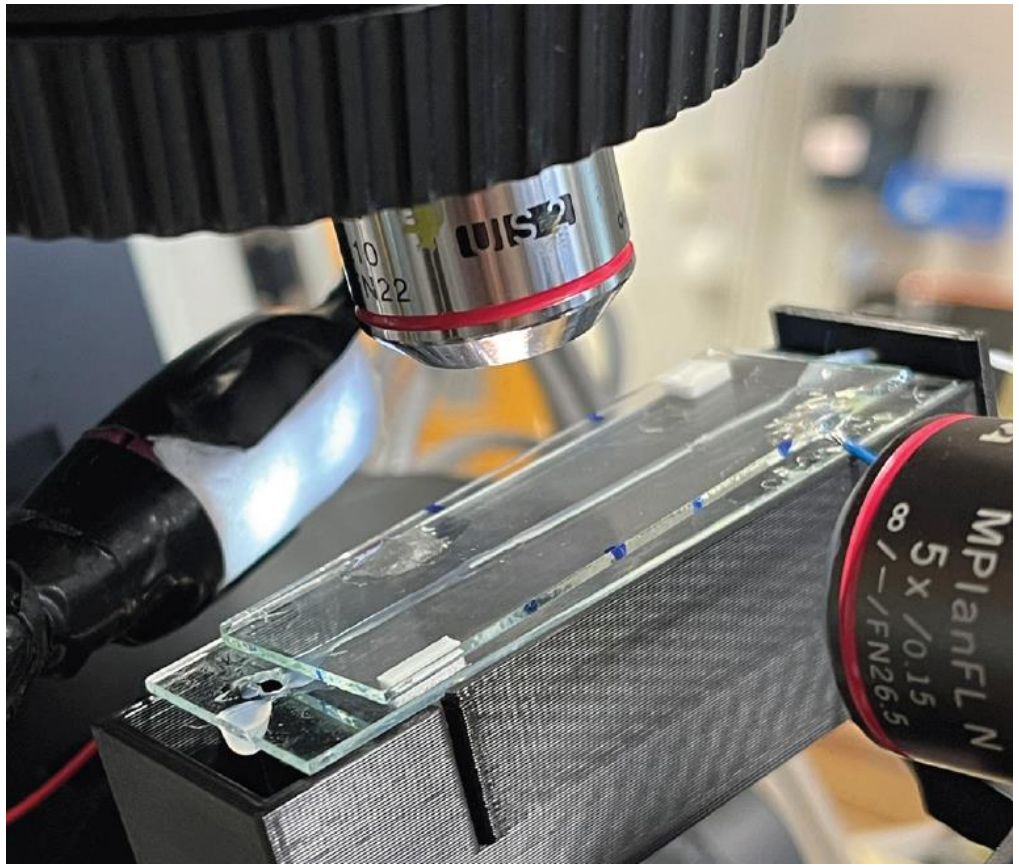

EXPERIMENTS

Our collaborators at Nottingham Trent University have brought this idea into reality:

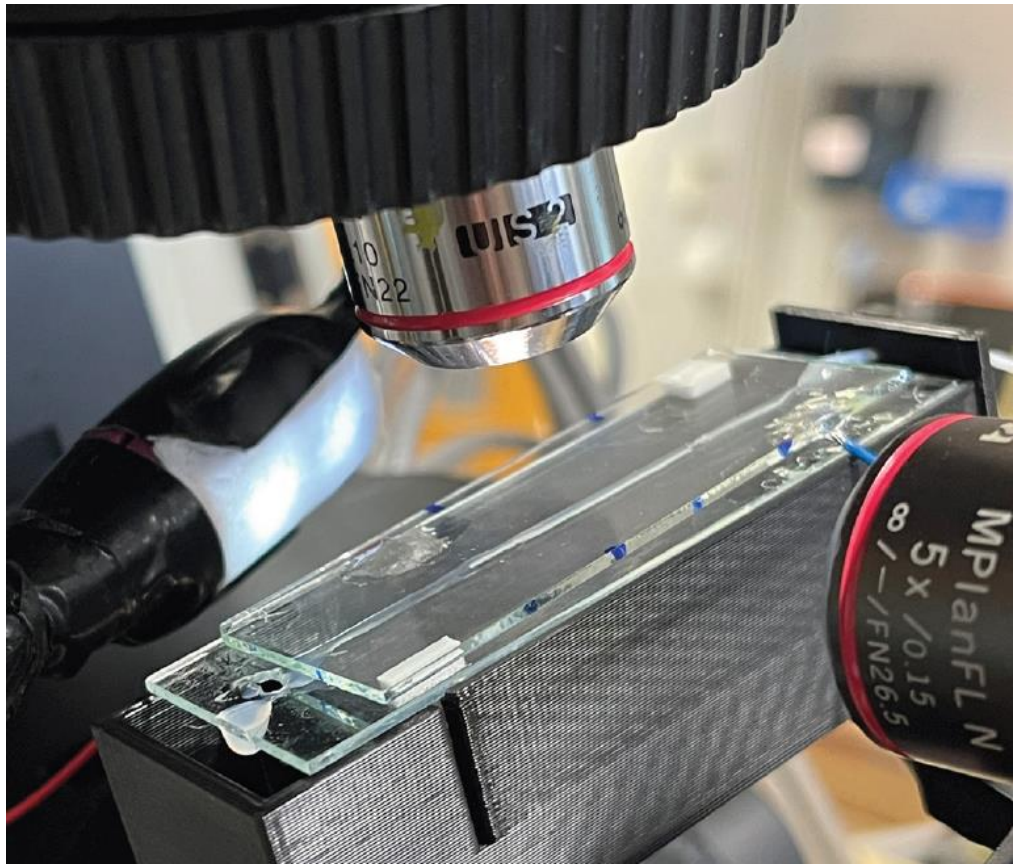

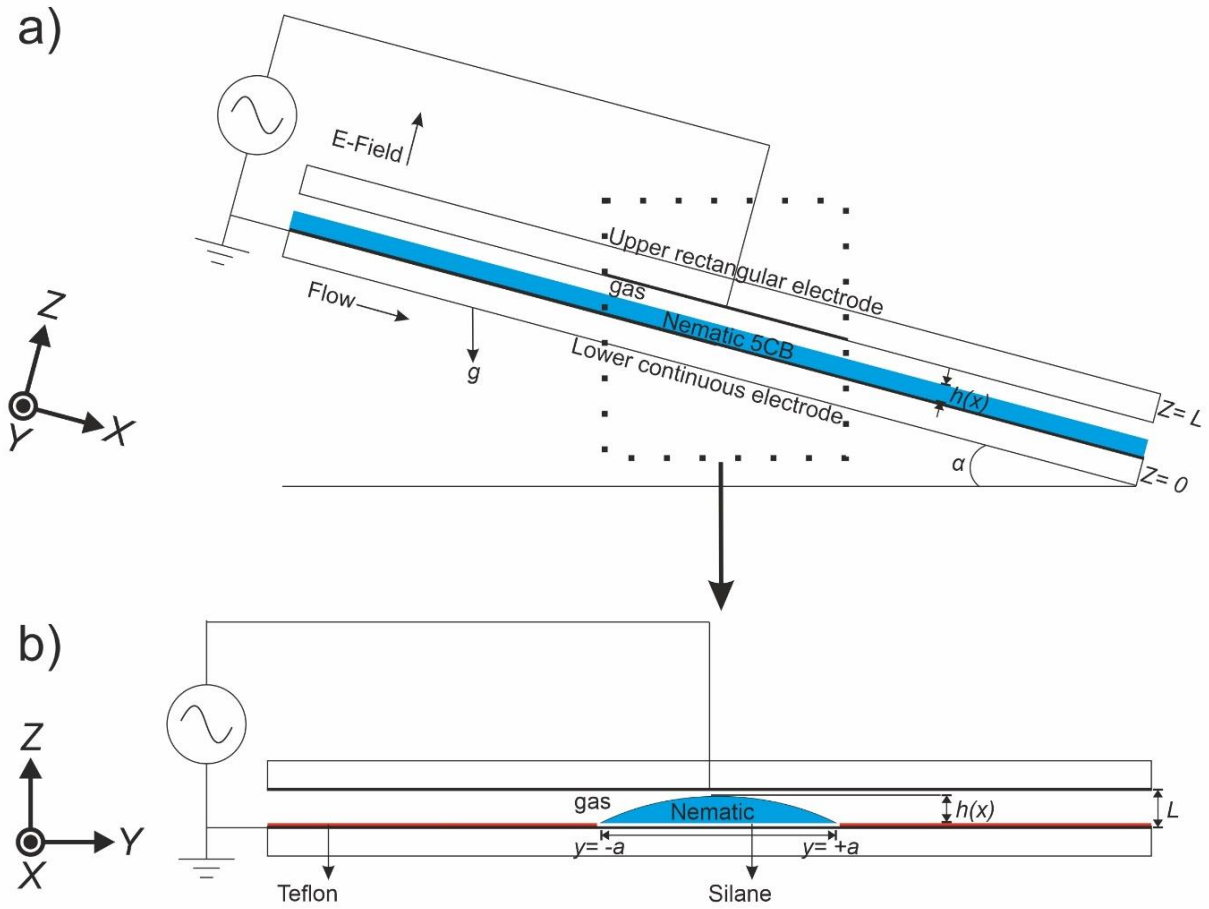

EXPERIMENTS

The rivulet height increases upon the application of voltage.

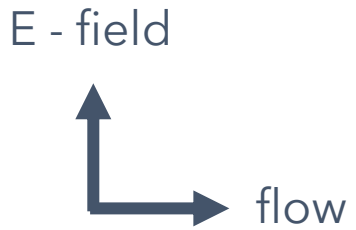

Q = 2000 nl/s

Q = 1000 nl/s

Q = 500 nl/s

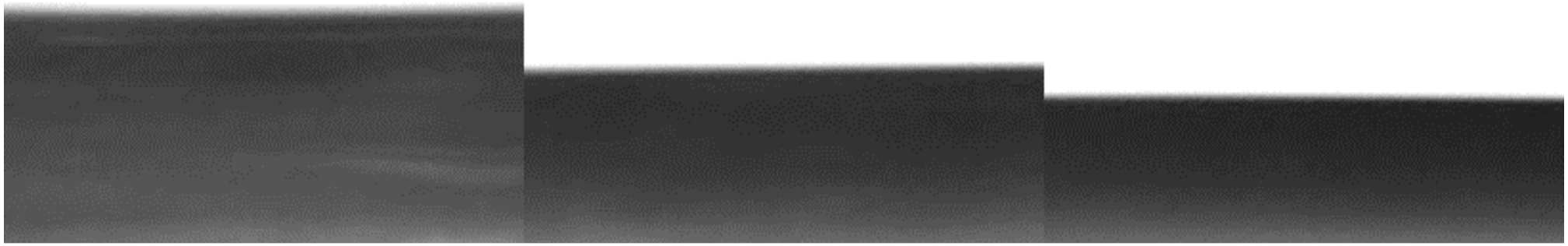

Increase in rivulet height on application of voltage (1000 V)

HOW CAN WE MODEL THESE EXPERIMENTS?

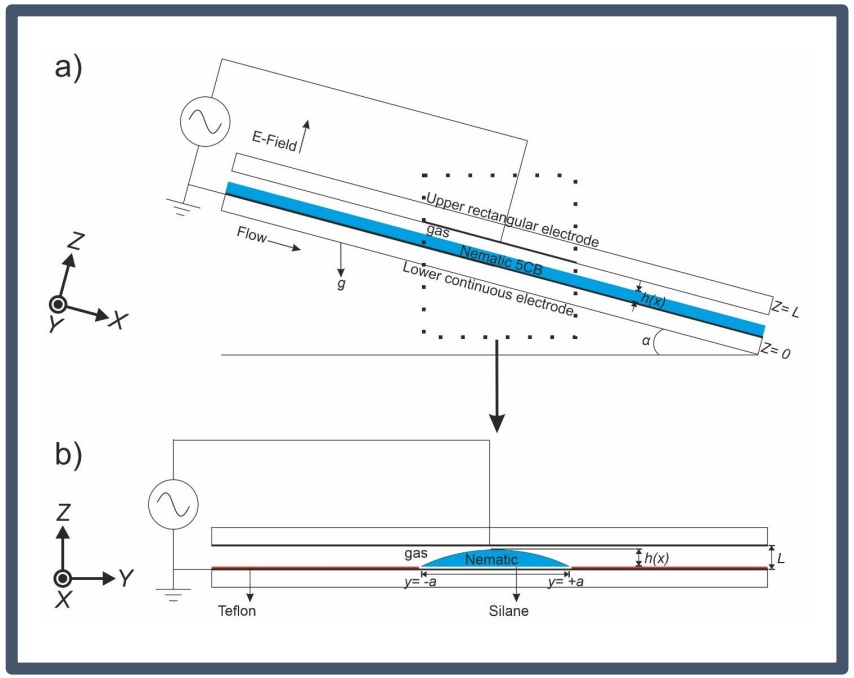

HOW CAN WE MODEL THESE EXPERIMENTS?

The electric field:

$$\nabla \cdot \boldsymbol{D}_{\mathrm{A}} = 0$$
$$\nabla \cdot \boldsymbol{D}_{\mathrm{N}} = 0$$

with

$$\boldsymbol{D}_{\mathrm{A}} = \epsilon_0 \epsilon_{\mathrm{A}} \boldsymbol{E}_{\mathrm{A}}$$

$$\boldsymbol{D}_{\mathrm{N}} = \epsilon_0 \epsilon_{\perp} \boldsymbol{E}_{\mathrm{N}} + \epsilon_0 \Delta\epsilon \left(\boldsymbol{n} \cdot \boldsymbol{E}_{\mathrm{N}} \right) \boldsymbol{E}_{\mathrm{N}}$$

Anchoring:

$$\frac{\partial W_{\mathrm{F}}}{\partial n_{i,j}} \nu_j + \frac{\partial \omega_{\mathrm{S}}}{\partial n_i} = \lambda n_i$$

with

$$\omega_{\mathrm{S}} = \gamma + \frac{C}{4} \left(1 - 2 \left(\boldsymbol{\nu} \cdot \boldsymbol{n} \right)^2 \right)$$

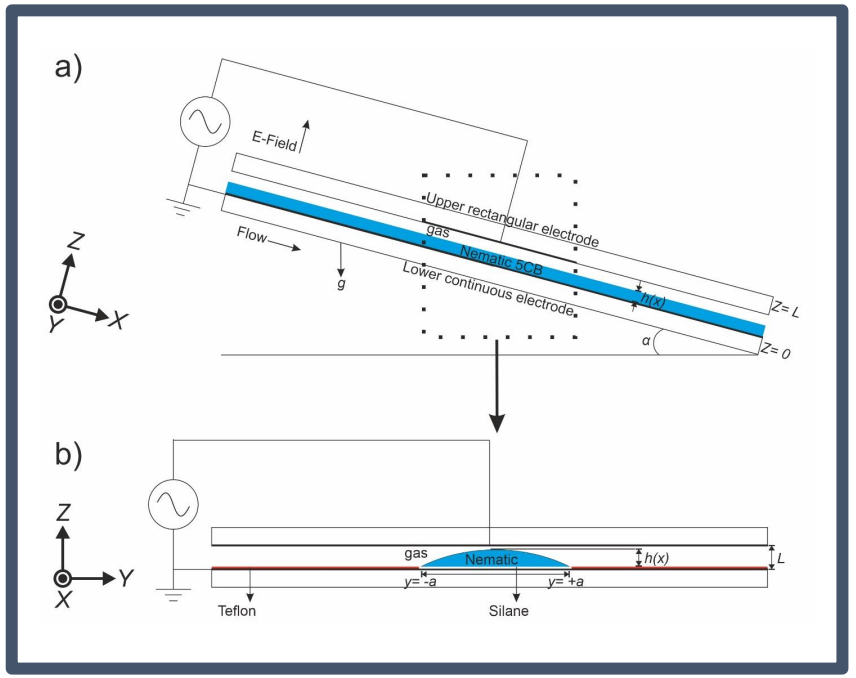

Ericksen-Leslie equations for the flow:

$$\rho \dot{u}_i = -\frac{\partial}{\partial x_i}(p + W_{\mathrm{F}}) + \tilde{g}_j n_{i,j} + \frac{\partial \tilde{t}_{ij}}{\partial x_j}$$

$$\lambda n_i = \tilde{g}_i + \frac{\partial W_{\mathrm{F}}}{\partial n_i} - \frac{\partial}{\partial x_j}\left(\frac{\partial W_{\mathrm{F}}}{\partial n_{i,j}} \right)$$

with

$$\tilde{t}_{ij} = \alpha_1 n_k e_{kp} n_p n_i n_j + \alpha_2 N_i n_j + \alpha_3 n_i N_j + \alpha_4 e_{ij} + \alpha_5 n_i e_{ik} n_k + \alpha_6 n_i e_{jk} n_k$$

$$W_{\mathrm{F}} = \frac{1}{2} K_1 (\nabla \cdot \boldsymbol{n})^2 + \frac{1}{2} K_2 (\boldsymbol{n} \cdot \nabla \times \boldsymbol{n})^2 + \frac{1}{2} K_3 (\boldsymbol{n} \times \nabla \times \boldsymbol{n})^2 + \frac{1}{2}(K_2 + K_4) \nabla \cdot \left[(\boldsymbol{n} \cdot \nabla)\boldsymbol{n} - (\nabla \cdot \boldsymbol{n})\boldsymbol{n} \right]$$

$$\tilde{g}_i = -(\alpha_3 - \alpha_2) N_i - (\alpha_3 + \alpha_2) e_{ip} n_p$$

Free surface effects (Young–Laplace equation):

$$p - p_{\mathrm{a}} - W - \psi + \gamma_{\mathrm{GN}} \frac{h_{yy}}{\left(1 + h_y^2\right)^{3/2}} + \frac{C_{\mathrm{GN}}}{4\left(1 + h_y^2\right)^{5/2}} \left[3 h_{yy} \left[\left(h_y^2 - 1\right) \cos 2\theta - 2 h_y \sin 2\theta \right] + \left(1 + h_y^2\right) \left(4 \cos 2\theta \left[\theta_y - h_y \left(1 + h_y^2\right) \theta_z \right] + 2 \sin 2\theta \left[\left(1 - h_y^4\right) \theta_z + h_y \left(3 + h_y^2\right) \theta_y \right] \right) \right] = 0$$

and BCs!

THE REDUCED MODEL

Under a standard thin-film rivulet approach used for a Newtonian rivulet [1,2] we obtain the following reduced model:

$$\mu_1(\theta) = \eta_1 \cos^2\theta + \eta_2 \sin^2\theta + \eta_{12} \sin^2\theta \cos^2\theta = \mu(\theta)$$

$$0 = \sin\alpha + (\mu_1(\theta) u_z)_z\,,$$

$$0 = -\tilde{p}_y + \left(\frac{\mathcal{V}}{\mathcal{U}} \mu_2(\theta) v_z\right)_z\,, \qquad \text{and} \qquad 0 = \frac{1}{2}(\gamma_1 + \gamma_2 \cos 2\theta)\, u_z + \frac{\epsilon_0 \Delta\epsilon\, I\, V^2}{\eta_3\, Q} \sin\theta \cos\theta\, U_z^2$$

$$0 = -\cos\alpha - \tilde{p}_z,$$

With the boundary conditions on the rivulet

$$\tilde{p} - p_a = -\gamma h_{yy}, \qquad Q = \int_{-a}^{a}\int_{0}^{h} u\,dz\,dy,$$

$$u = 0 \quad \text{on} \quad z = \upsilon,$$

$$u_z = 0 \quad \text{and} \quad v_z = 0 \quad \text{on} \quad z = h,$$

$$h = 0, \quad \text{and} \quad h_y = \mp\beta \quad \text{at} \quad y = \pm a.$$

Compare to the corresponding Newtonian eq.'s

$$0 = \sin\alpha + \mu u_{zz},$$

$$0 = -\tilde{p}_y + \frac{\mathcal{V}}{\mathcal{U}} \mu\, v_{zz},$$

$$0 = -\cos\alpha - \tilde{p}_z,$$

[1] Paterson, Wilson and Duffy. *Eur. J. Mech. B* **41**, 94-108, 2013

[2] Duffy and Moffatt. *J. Chem. Eng.* **60**, 141-146, 1995

SOLUTION TO THE REDUCED MODEL

The reduced model yields the following solution

$$u = \frac{\sin\alpha}{2\mu_1(\hat{\theta})}(2h - z)z, \quad v = 0, \quad w = 0, \quad p = -\frac{\partial^2 h}{\partial y^2} + \cos\alpha(h - z),$$

$$h = \left[\int_{-a}^{a} \frac{\sin\alpha}{3\mu_1(\hat{\theta})}\left(\frac{\cosh(ma) - \cosh(my)}{m\sinh(ma)}\right)^3 \mathrm{d}y\right]^{-1/3} \frac{\cosh(ma) - \cosh(my)}{m\sinh(ma)}.$$

$$0 = \frac{\gamma_1 + \gamma_2\cos 2\hat{\theta}}{4\mu_1(\hat{\theta})}h + \frac{\epsilon_0\,\Delta\epsilon\,I\,\mathbb{V}^2}{\sin\alpha\,\eta_3\,Q}\frac{\sin\hat{\theta}\cos\hat{\theta}}{\left((\epsilon_\perp + \Delta\epsilon\sin^2\hat{\theta})(H - h) + h\right)^2}.$$

SOLUTION TO THE REDUCED MODEL

The reduced model yields the following solution

$$0 = \frac{\gamma_1 + \gamma_2 \cos 2\hat{\theta}}{4\mu_1(\hat{\theta})}\, h + \frac{\epsilon_0\, \Delta\epsilon\, l\, \mathbb{V}^2}{\sin\alpha\, \eta_3\, Q} \frac{\sin\hat{\theta}\cos\hat{\theta}}{\left((\epsilon_\perp + \Delta\epsilon \sin^2\hat{\theta})(H-h) + h\right)^2}.$$

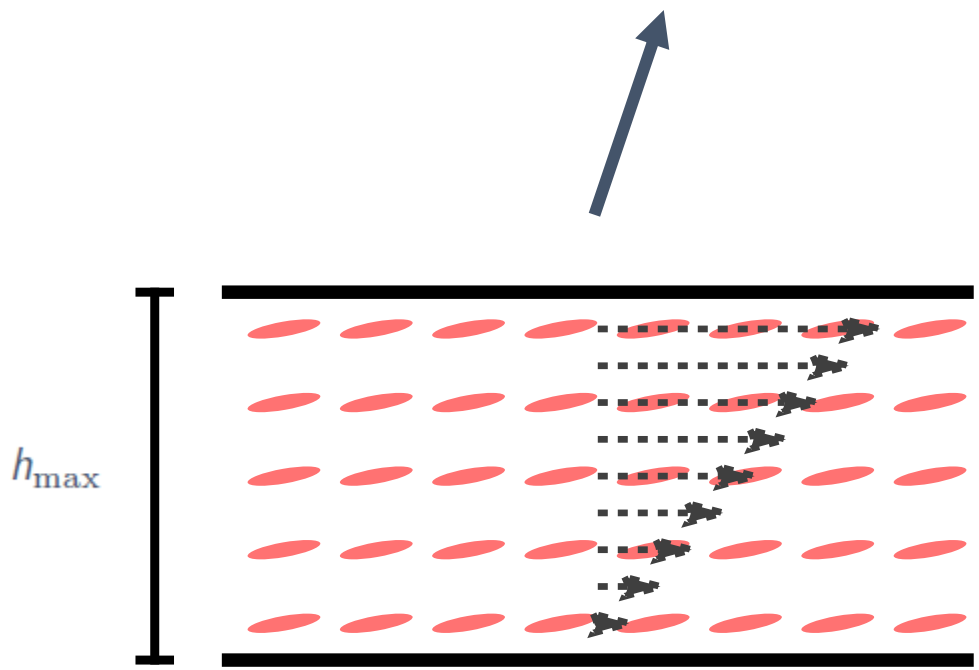

nematic rivulet – **field off**

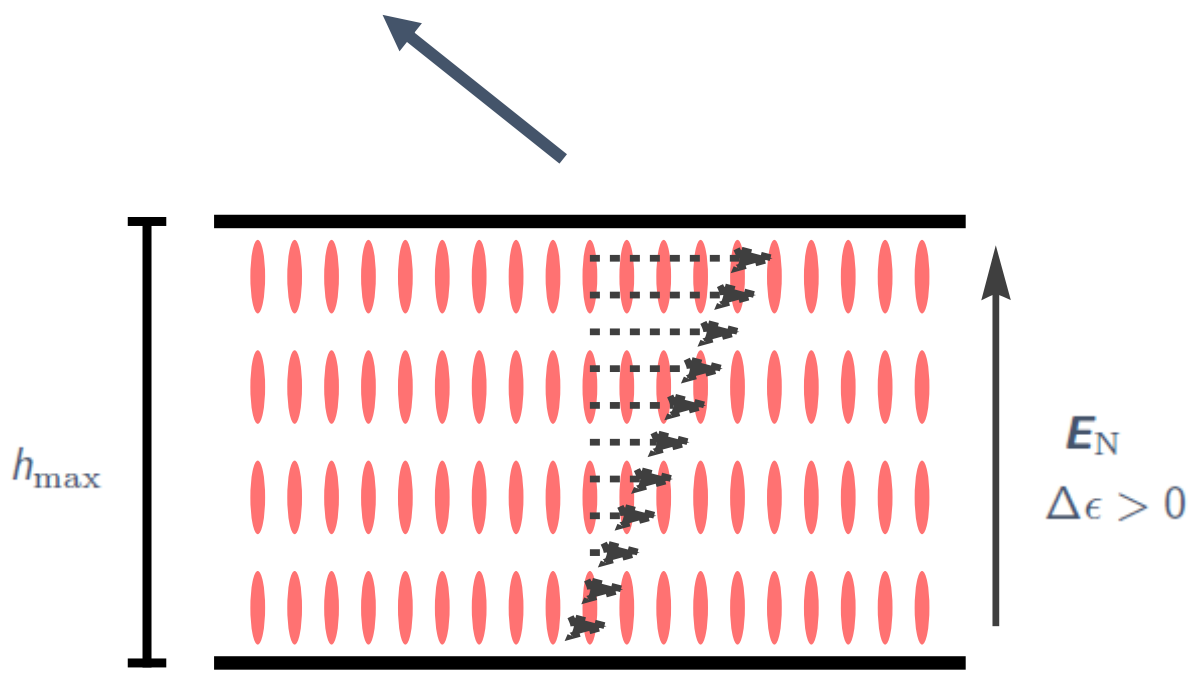

nematic rivulet – **field on**

REDUCED MODEL SOLUTIONS

Under the reduced model, solutions can be obtained for *h*, *p* and *u*:

Q = 500 nl/s and V = 10 V

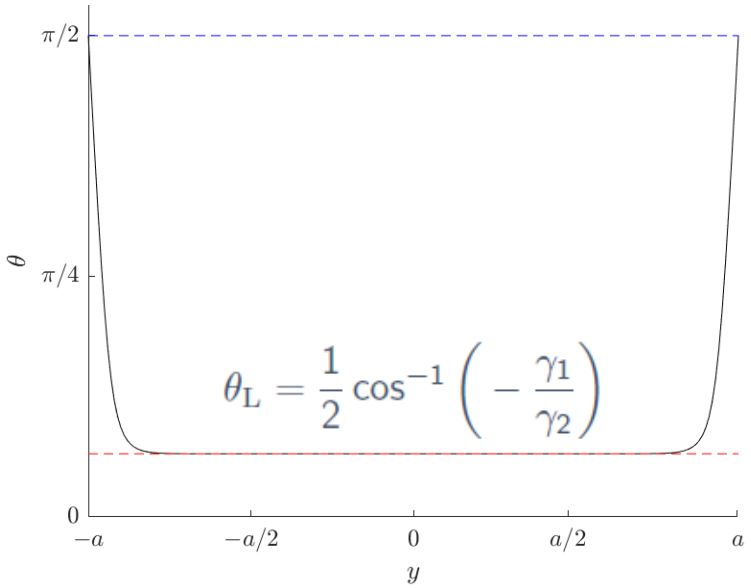

director angle

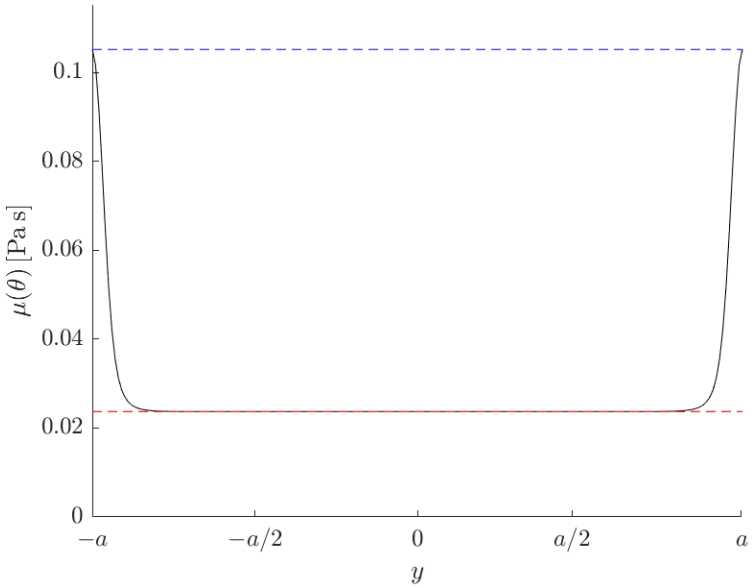

effective viscosity

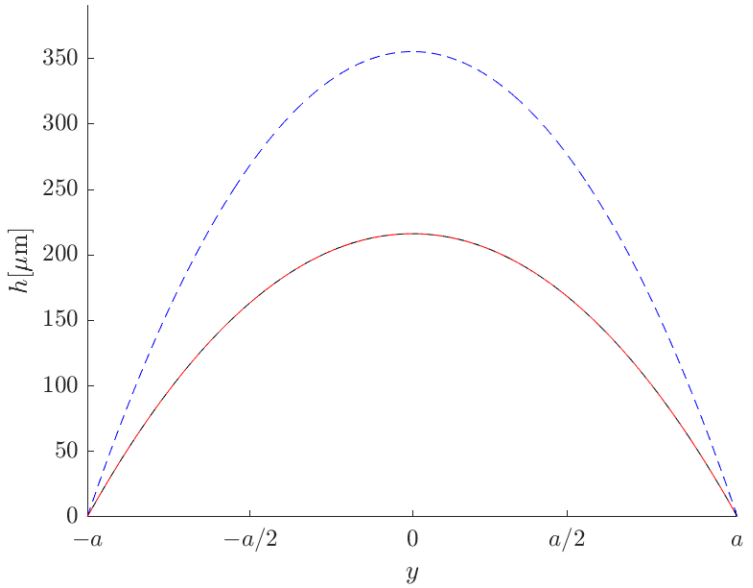

height of the rivulet

REDUCED MODEL SOLUTIONS

Under the reduced model, solutions can be obtained for *h*, *p* and *u*:

Q = 500 nl/s and V = 800 V

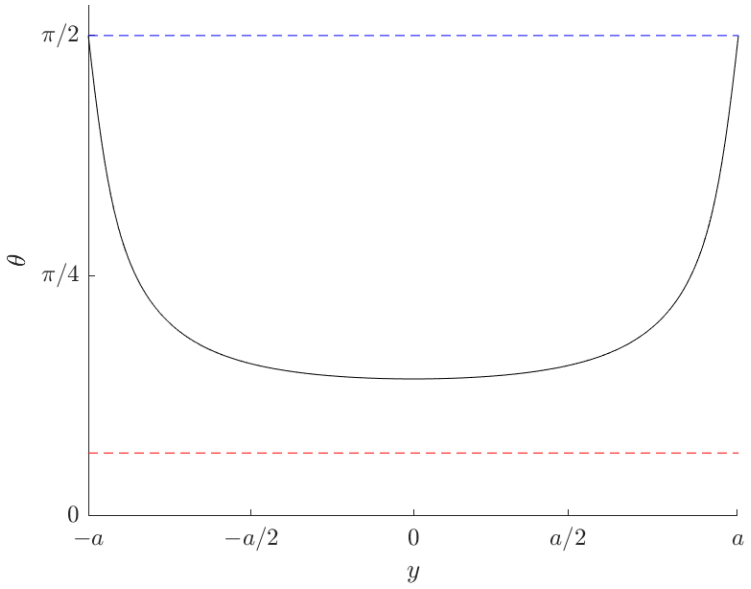

director angle

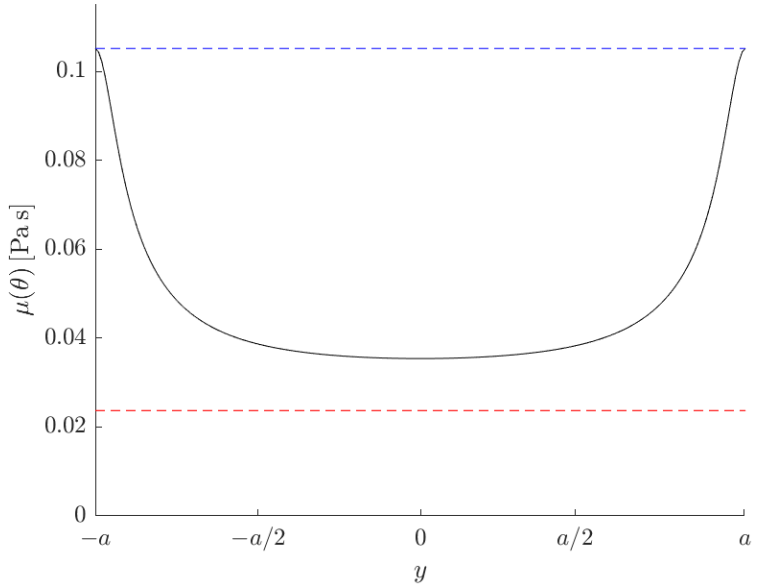

effective viscosity

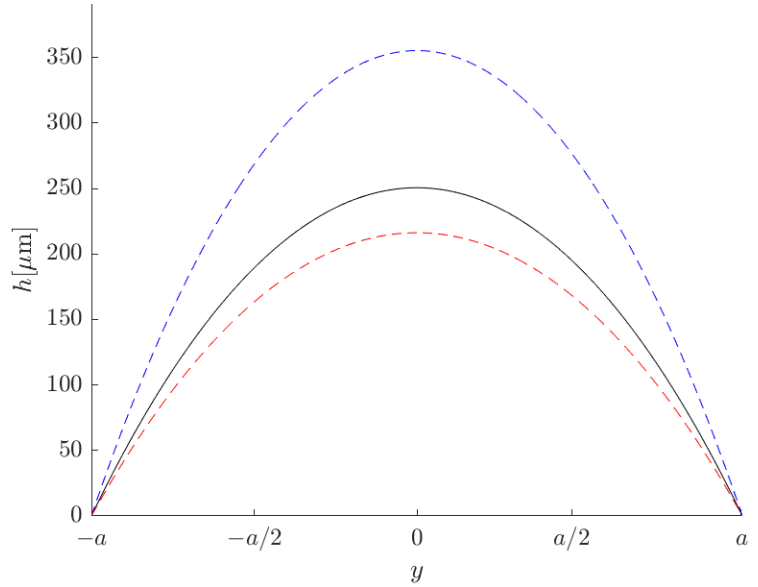

height of the rivulet

REDUCED MODEL SOLUTIONS

Under the reduced model, solutions can be obtained for *h*, *p* and *u*:

Q = 10 nl/s and V = 1000 V

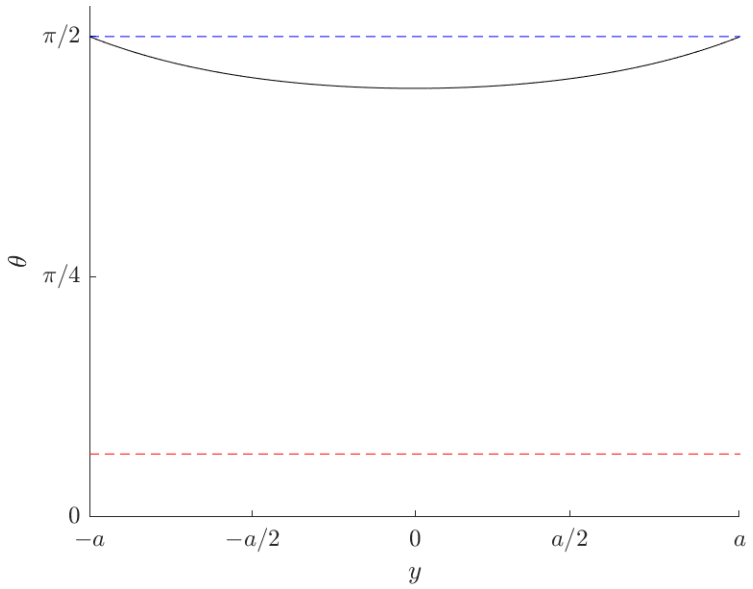

director angle

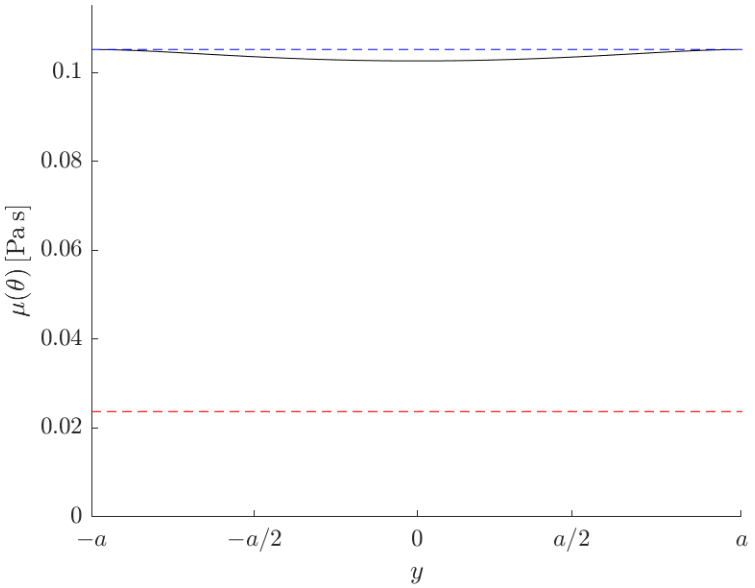

effective viscosity

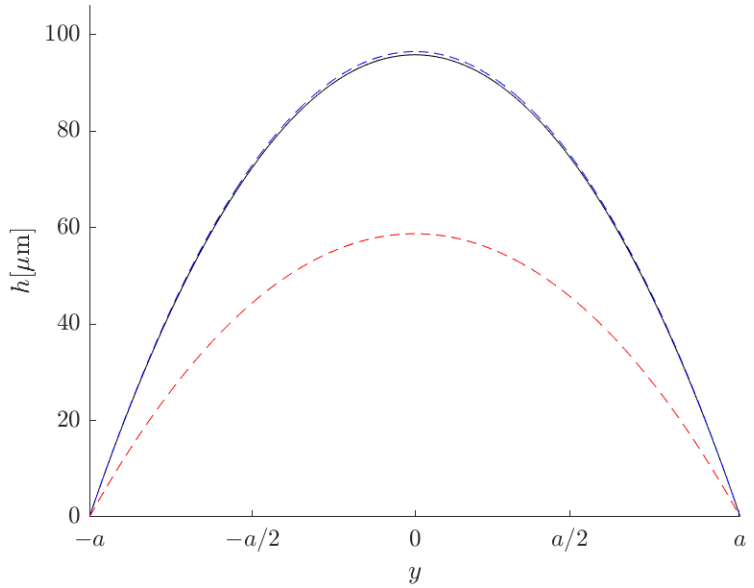

height of the rivulet

COMPARISON WITH EXPERIMENT

The reduced model is used to compare with the experiments.

For the voltages V=1000 V and V = 0 V a range of prescribed fluxes (Q) are sampled in the experiments.

The grey regions account for possible errors in the experiment. The solid and dashed lines are the best fit in these regions.

The model is successful in capturing the behaviour of the experiments.

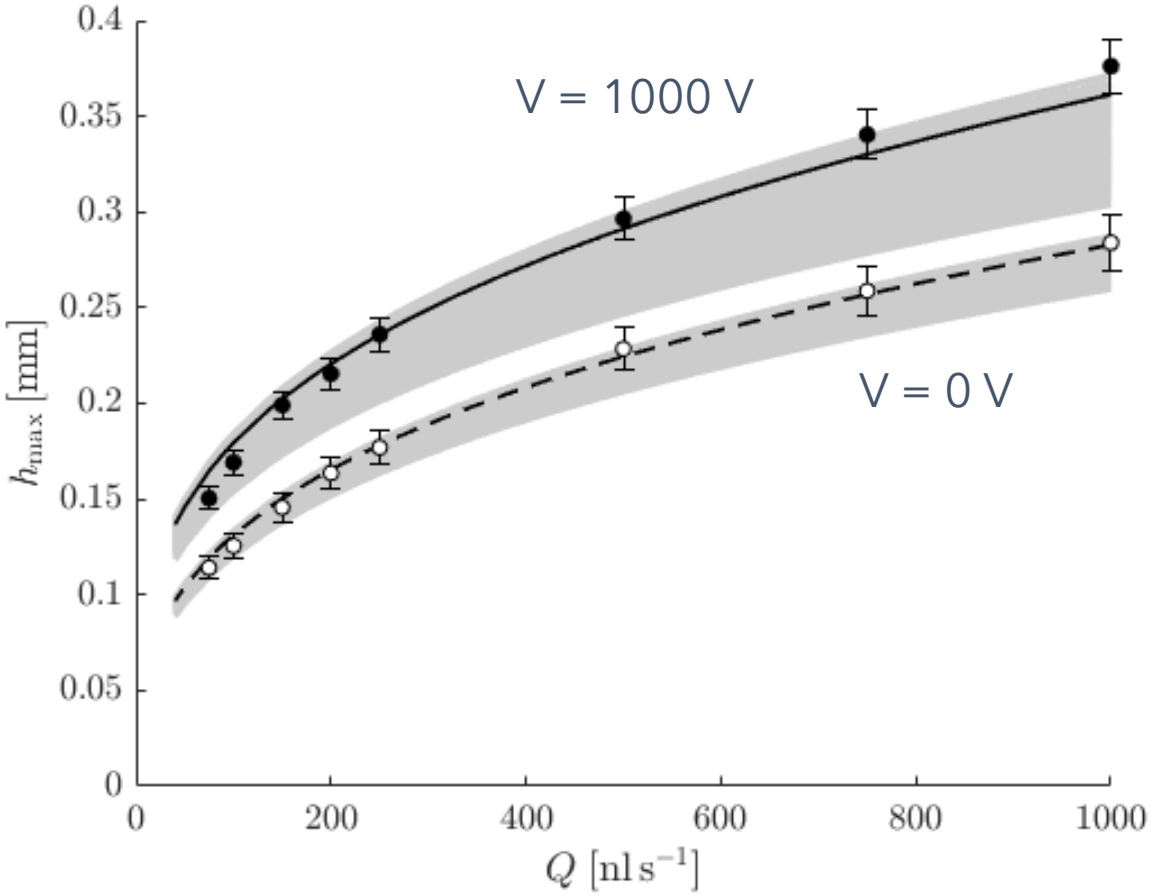

CONCLUSIONS

We have considered the control of a nematic liquid crystal rivulet with an applied electric field.

Under a number of assumptions, the Ericksen–Leslie equations and Gauss' law for the electric displacement field reduced to a model that describes the balance of flow and field alignment in the nematic rivulet.

The physics behind this process is simple:

- the director orientation is controlled by the application of an electric field,
- rotation of director changes the effective viscosity of the rivulet,
- an increase in the viscosity increases the height and decreases the velocity.

The naive model performs well in comparison to the experiments.

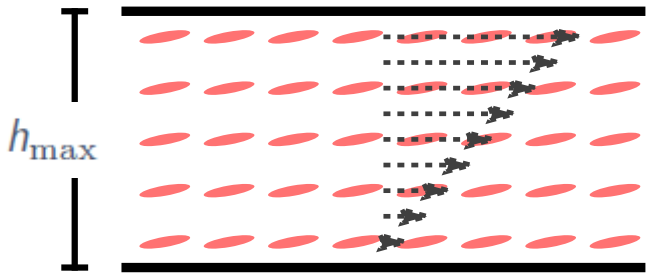

Flow aligning

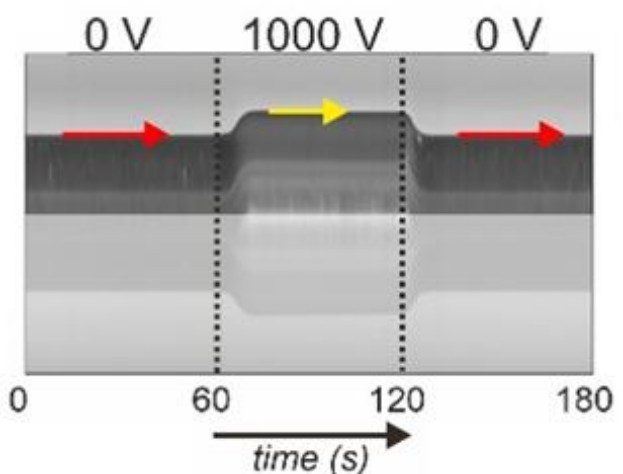

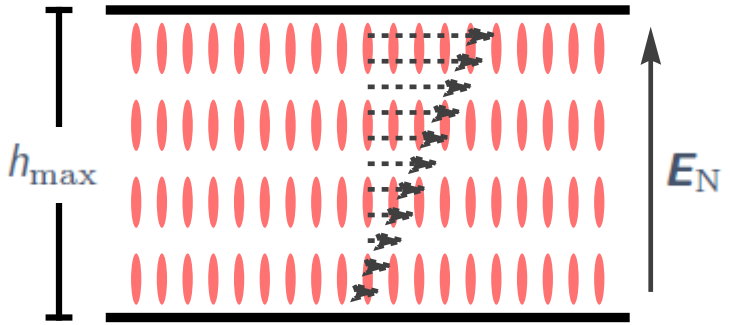

Field aligning